

Experimental characterization of the in-plane shear strength of
unreinforced masonry walls with damp-proof course and thermal break layer

Peer-reviewed author version

DRAGAN, Dan; DAS, Rajarshi; VANHEUKELOM, Martijn; VANDOREN, Bram &
DEGEE, Herve (2024) Experimental characterization of the in-plane shear strength
of unreinforced masonry walls with damp-proof course and thermal break layer. In:
Journal of building engineering, 98 (Art N° 111314).

DOI: 10.1016/j.jobe.2024.111314

Handle: <http://hdl.handle.net/1942/44753>

Experimental characterization of the in-plane shear strength of unreinforced masonry walls with damp-proof course and thermal break layer

Dan Dragan^a, Rajarshi Das^{a,1}, Martijn Vanheukelom^a, Bram Vandoren^a, Hervé Degée^a

^a Construction Engineering Research Group, Faculty of Engineering Technology, Hasselt University, Hasselt, Belgium

Abstract

Due to the highly demanding energy standards in Europe and challenging weather conditions, thermal break elements, such as aerated autoclaved concrete (AAC), have become increasingly popular in modern day residential buildings made of masonry cavity walls. Furthermore, a damp-proof course (DPC) layer is also used on top of the thermal break element to prevent water seeping and eventual entrapment due to capillary action. The presence of an AAC layer and of a DPC can have an adverse effect on the in-plane shear strength of a masonry wall, although information on this is barely available in the existing literature. This study aims at filling that knowledge gap through experimental investigations on traditional masonry walls and composite masonry walls, i.e. with an AAC and a DPC layer. The in-plane shear behaviour is compared between both types of wall specimens on the base of load-displacement curves and observation of failure modes. The capacity of analytical design approaches in predicting the test results has also been assessed. For the tested configurations, it can be concluded that the presence of AAC and DPC makes the failure mode switch from diagonal shear sliding combined with flexural toe crushing to horizontal shear sliding with crushing localized in the AAC layer, associated to a drop of the resistance by 6 to 9% depending on the type of clay units and mortar. The proposed analytical method, derived from EN 1996-1-1, is providing a safe estimate of the test results with a similar level of accuracy for traditional and composite configurations (predicted values in the range of 75 to 86% of the measured values). Finally, the influence of the definition of the compressed length and of the shear span ratio are shortly discussed.

Keywords: Autoclaved Aerated Concrete (AAC), Damp proof course (DPC), Composite masonry wall, In-plane shear resistance, Experimental shear tests.

¹ corresponding author, e-mail address: rajarshi.das@uhasselt.be; Address: Universiteit Hasselt - Campus Diepenbeek, Kantoor ACB² 1.4, Applicatiecentrum beton en bouw, Wetenschapspark 34, 3590 Belgium

List of symbols and abbreviations

Symbols			
e	Eccentricity between wall central axis and the axis of the reaction force	$V_{Rd,f}$	Shear force corresponding to M_{Rd} , shear span = 1.0
f_b	Normalized compressive strength of masonry units	$V_{Rd,s1}$	In-plane resistance to sliding shear
f_d	Design compressive strength of masonry	$V_{Rd,s2}$	In-plane resistance to diagonal shear
f_k	Characteristic compressive strength of masonry	$V_{Rd,u}$	Ultimate in-plane shear resistance
f_{v0}	Mean initial shear strength	Φ	Reduction factor
f_{vd}	Design shear strength of masonry	γ_M	Partial safety factor for material
f_{vk}	Characteristic shear strength of masonry	μ_f	Characteristic friction coefficient
f_{vk0}	Characteristic initial shear strength of masonry	η_f	Factor defining the eqv. rectangular stress block
f_{vit}	Limiting value of f_{vk}	σ_0	Applied compressive stress
h	Height of masonry wallette	σ_d	Design compressive stress
h_u	Height of masonry unit		
K_0	Initial stiffness of masonry wallette		
l	Length of masonry wallette		
l_c	Length of compressed (contact) part of the wallette		
l_{c_linear}	Length of compressed (contact) part assuming a linear stress distribution		
$l_{c_uniform}$	Length of compressed (contact) part assuming a uniform stress distribution		
$l_{c_discrete}$	Length of compressed (contact) part assuming discrete masonry units		
l_u	Length of masonry unit		
M_{Ed}	Moment corresponding to V_{Ed}		
M_{Rd}	Design moment resistance		
N_{Ed}	Design compression load		
R^2	Coefficient of determination		
R_{Ed}	Reaction at compressed part of the wall		
t_u	Thickness of masonry unit		
t	Thickness of masonry wallette		
V_{Ed}	Design shear load		
V_{exp}	Peak shear resistance obtained from experiments on each masonry wallette		
$V_{exp,avg}$	Average of experimental peak experimental shear resistance values		
V_{Rd}	Design in-plane shear resistance		
		Abbreviations	
		A	Autoclaved aerated concrete unit
		AAC	Autoclaved aerated concrete
		DPC	Damp proof course
		DSS	Diagonal shear sliding
		HSS	Horizontal shear sliding
		G	Thin layer mortar
		GPM	General Purpose mortar
		N	General purpose mortar
		P	Clay brick with tongue and groove
		SS	Shear sliding
		T	Clay brick without tongue and groove
		TC	Toe crushing
		TLM	Thin layer mortar

1. Introduction

Masonry construction is quite popular for residential use in low- to medium-rise buildings due to its high durability, resistance against vertical loads and an effective construction cost [1]. It is often characterized as a composite construction material, primarily consisting of individual masonry units and mortar. The masonry units can be made of different raw materials (natural or artificial) such as stones, calcium silicate, clay and concrete aggregates, whereas the mortar is either made of glue or is simply a mixture of cement, sand, lime and additives in water. Three types of mortar are commonly used in practice: (i) general-purpose mortar (GPM) – with a joint thickness of 6-15 mm, (ii) thin layer mortar (TLM) – with a joint thickness of 0.5-3 mm, and (iii) lightweight mortar – having a joint thickness of 8-15 mm [2]. A set of European standards has duly been developed and consistently updated to regulate different aspects of masonry constructions in real-life, e.g. EN 772-1 [3] controls the material characteristics of masonry units, EN 1052-1 [4] defines the testing method to characterize the resistance of masonry walls, EN-1996-1-1 [5] controls the structural application of masonry structures, etc.

However, in the last few years, the thermal performance of residential buildings has gained quite a lot of attention all around Europe and particularly in the north and north-western areas, due to environmental challenges. The European Energy Directive has considered numerous guidelines and standards to enhance the thermal performance [6] of residential buildings, which are mostly masonry structures. The European Commission has set out rules for the general public: all new buildings should follow zero- or low-energy consumption [7], where a “low-energy” house in Belgium is officially defined as a house in which the total energy demand for space heating and cooling is less than or equal to 30 kWh/m² heated net floor area. Standard “zero-energy” houses should include thicker layers of insulation, airtight interior finishes, energy-efficient ventilation, passive solar energy-efficient heating, alternative energy sources, and, most importantly, the absence of thermal bridges. As a result, more and more building systems have moved on from single monolithic walls with large thicknesses to a cavity wall with air spaces, with additional insulating layers and thermal break elements to satisfy the thermal requirements.

A thermal break element (see Fig. 1) has proven to be necessary to limit thermal bridges. The most common examples of a load-bearing thermal break element used in today’s construction industry are autoclaved aerated concrete (AAC), cellular glass and polystyrene block insulation. Some of these elements have been studied individually to characterize their mechanical properties while others have been studied with a combination of masonry units to understand their possible influence on the overall performance of a structure [8-22]. For instance, compression and splitting tests were done by Malyszko [8] on AAC cubes and cylinders to determine their tensile behavior and elastic modulus. Ferretti et al. [9] conducted monotonic (uniaxial and biaxial) tests on short AAC masonry panels and three-point bending tests on AAC masonry beams to characterize the mechanical properties of AAC. The authors highlighted a relatively isotropic behavior for the AAC material, with a limited compressive strength of 3.1 MPa (on a cube with 100 mm edge length), and a very low stiffness ($E = 1300$ MPa). Memari [10] compared the lateral response of AAC wallettes under in-plane shear and out-of-plane loads with traditional concrete and adobe wallettes. Overall, these studies confirmed that the AAC possess a lesser bearing capacity compared to the traditional masonry units. Jasinski [20-21] investigated 18 confined masonry walls made of AAC units and compared them with unconfined masonry walls (referenced models). The author proposed a modified bilinearization method to characterize the masonry wall behaviour and documented the procedure to verify the shear load capacity by means of the shear-axial force interaction diagram drawn as per EN-1996-1-1 [5]. The influence of the wall shape and the vertical load eccentricity was also assessed corresponding to the shape of the

interaction diagram. Martens studied the mechanical strength behavior of cellular glass units under eccentric and non-eccentric load conditions [22]. He also conducted tests on medium-scale composite masonry walls under uniaxial compression to evaluate their structural strength in terms of compressive resistance. These composite walls were built with cellular glass units at the bottom layer combined with solid calcium silicate units, solid clay units, or perforated clay units at the upper layer. The cellular units were characterized by a limited bearing strength, with compressive strength ranging from 2.5 to 3.2 MPa. The author highlighted the fact that, both the thermal layer and the masonry units have a direct impact on the global compressive strengths of the wallets.

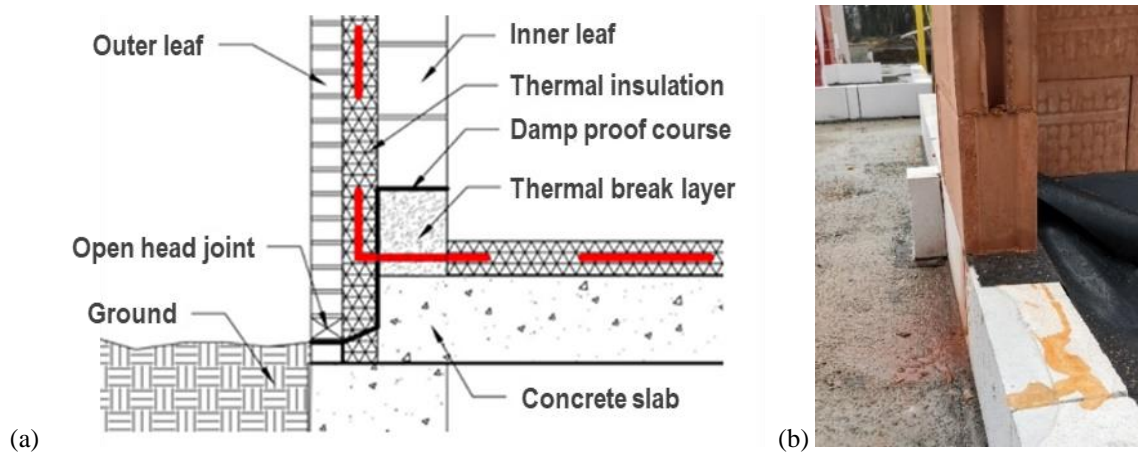


Figure 1. (a) Cut-out view and (b) picture of a typical clay masonry wall with thermal break layer and DPC.

Damp-proof course (DPC) layers are often used in masonry buildings to prevent water seepage through the outer leaf of the wall, which eventually gets trapped in the AAC. They are generally placed at the surroundings of a thermal break layer, embedded in the mortar joint, as shown in Fig. 1. However, the presence of a DPC layer can weaken the joint due to its inherent lack of shear and tensile strength. It is therefore important to assess the structural performance of the DPC and its influence on the overall masonry wall's performance, particularly under in-plane shear loading. Previous research on the use of DPC in masonry structures has mainly focused on the behavior of various DPC membranes under static, static-cyclic, and dynamic loads [23-28]. Griffith and Page [23] conducted monotonic, static-cyclic, and dynamic shear tests on small masonry elements (triplets) with different DPC membranes, such as bitumen-coated aluminium, polythene/bitumen-coated aluminium, and embossed polythene. They also reported the corresponding friction coefficients. The DPC membranes were placed in both mortar joints of the triplet, and in one series, the middle brick was made of concrete to simulate a concrete slab. The specimens were pre-compressed at a constant level during testing, with the load applied in the out-of-plane direction. The masonry materials consisted of extruded clay bricks and standard 1:1:6 (cement: lime: sand) mortar. The tests showed that shear can be transmitted through joints containing a DPC, with a reasonable hysteretic behavior. Additionally, no joint degradation occurred even after fifty load cycles. Similar findings were reported by Suter and Ibrahim [27], and Zhuge and Mills [28], the latter also conducting tests on six unreinforced clay brick wallets with built-in DPCs. Petrovic [29] and Vogeli [30] investigated the shear behaviour of unreinforced masonry (URM) walls with a soft-layer bed joint and a damp-proof course under lateral loads. The soft-layer acted as a weak plane, instigating horizontal sliding prior to any failure in the surrounding areas of the wall. It also showcased a great amount of plastic deformation prior to any shear failure of the masonry wall.

The foretold studies offer a significant collection of research data on the structural response of individual thermal break elements and DPC layers. But unfortunately, a lack of knowledge remains prevalent when it comes

to the combined or composite behaviour of a masonry wall build up with more than one type of masonry unit i.e. different types of clay bricks, different types of mortar, thermal break element (AAC) and DPC. Although the individual elements are separately covered by the current design standards e.g. EN-1996-1-1 [5], open questions are still present regarding their combined application. Furthermore, as the composite behaviour is quite complex, it often requires additional experimental tests to validate the corresponding theoretical and/or numerical models [31-33]. In order to address this issue, Deyazada et al. [34] took a first step in 2021, by investigating the compressive resistance of composite masonry walls comprising of two types of masonry units (clay and concrete), AAC as a thermal break element and a damp-proof course (DPC), under eccentric and non-eccentric vertical loads. Numerical and experimental studies were documented where the results showed an improvement of the compressive strength compared to a homogeneous wall made of only the weakest material. Different failure modes were noted in presence of the AAC and DPC. A good understanding was provided on the AAC's and DPC's influence on the overall structural performance and stability under vertical/compression loading scenarios. Certain indications on the global behaviour of composite masonry walls under compression loading has subsequently been recommended by the latest version of EN 1996-1-1 [5]. However, the shear and flexural behavior of such composite walls should also be studied to effectively design them in reality.

To that purpose, this research study aims at characterizing the in-plane shear behaviour of unreinforced masonry (URM) load-bearing walls which are essentially composite in nature, i.e. made of perforated clay bricks with and without tongue and groove vertical joints and including AAC as a thermal break layer and DPC. The clay bricks without tongue and groove are used in conjunction with general purpose mortar (GPM) and filled head joints whereas the clay bricks with tongue and groove are used together with thin layer mortar (TLM) and unfilled head joints. The scope of the study is essentially to evaluate the shear performances under static or quasi-static loads, typically relevant for designing horizontally resisting global systems against static wind load (i.e. "bracing" systems). The cyclic shear behaviour, as relevant for the seismic analysis and design, is not considered.

As no relevant experimental tests on the shear behaviour of composite walls including a DPC have been identified in the literature, the specific objectives of this pioneering study are (i) to perform a series of comparative monotonic tests to identify the differences between classical homogenous masonry walls and composite walls in terms of activated failure modes, achieved resistance and post-peak behaviour, and (ii) apply the analytical methods currently available in EN 1996-1-1, as recommended for the shear resistance of homogenous masonry, to composite walls, in order to evaluate their capacity in predicting the experimental resistance. It is however clear that, given the moderate number of specimens tested, the present study does not claim to provide definitive conclusions but rather to propose an initial assessment of the presence the AAC layer and DPC on the shear performances, similarly to what the same authors did in [34] for the compression performances. In order to achieve first conclusions, an arbitrary scope has therefore been chosen, in terms of size and shape of the wallettes, initial compression, shear span ratio and material selection.

More specifically, experimental tests have been conducted on four different types of composite wallettes to investigate the following aspects: (i) the in-plane shear resistance and failure mechanism of composite masonry including AAC and DPC, (ii) the influence of the AAC in terms of weakening the wall due to its lower bearing capacity (i.e. compressive strength), (iii) the definition of design procedures for such composite walls, with reference to the existing standards. The experimental results are therefore further compared with the analytical provisions recommended by the European standards, to characterize the suitability of the analytical models in

designing such composite masonry structures. The following sections provide respectively a summary of the materials used in the test campaign, experimental test set-up and instrumentation, experimental force-displacement curves and failure modes and finally the analytical assessment of the test results.

2. Materials, test set-up and instrumentation

2.1. Materials

Two types of clay units were used to build the wall specimens, i.e. perforated elements with and without tongue and groove. Such units are representative of the elements used in North-Western Europe for modern load-bearing masonry. Solid bricks are not considered as they are mainly used as facing elements. Each type of masonry units used in the experimental studies (see Fig. 2) was taken from a same batch to have consistent material properties. The perforations in the clay bricks had a 47% void ratio, identifying as group 2 units according to Table 5.1 of EN 1996-1-1 [5]. The specimens were built by skilled masons in the laboratory on prefabricated reinforced concrete lintels. The head joints of the clay bricks with TLM were not filled but had a tongue and groove system. The average thickness for TLM was 1 mm. The joints of the clay bricks with GPM had an average thickness of 12 mm and were flush pointed on one side, so as to perform an optical measurement using Digital Image Correlation (DIC).



Figure 2. Masonry units used in experiments: (a) clay brick for GPM, (b) clay brick for TLM, (c) AAC block.

Prior to the global in-plane shear tests on the URM wallettes, a total no. of 138 triplet tests were performed considering three different pre-compression levels, to determine the initial shear strength and friction angle according to the EN 1052-3 provisions. A comprehensive description on the experimental investigations have been published by the authors in a previous scientific article [35]. The material properties relevant to this particular study are summarized below to offer fundamental clarity on the different units used in the wallettes: (i) The dimensions and mean compressive strength of the individual masonry units are listed in Table 1 with their corresponding abbreviations. The “T” type masonry unit is a Wienerberger Thermobrick 10N “Nova” with two larger holes and without tongue and groove [36]. The “P” type masonry unit is a Wienerberger Porotherm PLS 500 15N clay brick with tongue and groove [37]. The mean density of both “T” and “P” clay bricks at dry conditions are 850 kg/m^3 . The mean density of the AAC blocks in dry conditions is 489 kg/m^3 . The moisture content was however not measured. Approximately 14 litres of M5 GPM was prepared using 3.25 litres of pure water per 25 kg of dry mortar, to realise a compressive strength of 8 MPa after 28 days, with a water absorption $\leq 0.40 \text{ kg}/(\text{m}^2\text{min}^{0.5})$, adhesion $\geq 0.15 \text{ N/mm}^2$. A Porotherm lime mortar is used as TLM, adding 6.5-7.5 litres of water per 25 kg of powder (3 minutes mixing followed by 2 minutes resting period). The adhesion of the TLM is 0.6 N/mm^2 ; (ii) Table 2 summarizes the different types of triplets investigated under 3 different pre-compression

levels (three tests per pre-compression level), with their mean initial shear strength, mean friction coefficient and coefficient of determination (R^2). The reference name of each triplet has the format $X_1X_2X_3X_4$, where X_1 represents the clay bricks on the outside layers (T or P), X_2 represents the masonry unit in the middle layer (T, P or A), X_3 represents the mortar type (N or G) and X_4 indicates the use of a DPC layer (D). Three different failure modes were obtained from the triplet tests: sliding of the joints (see Fig. 3a), crushing (pore collapse) of the bricks (see Fig. 3b), or a combination of both (see Fig. 3c). The failure modes associated to each individual triplet test can be found in [35]. It was noted that, the maximum shear stress of the specimens decreases with the presence of an AAC block and even more with a DPC layer. The optimum position of the DPC layer was found to be the middle of a mortar joint, i.e. “sandwiched”. However, The Mohr–Coulomb curve could not be drawn for the PPG specimens as the samples did not fail in sliding but a combination of crushing (i.e., pore collapse of the center unit) and sliding, even at very low pre-compression levels [35]. (iii) Table 3 summarizes the geometric dimensions of the wallettes (corresponding to the triplet specimens) investigated in this study under global in-plane shear loads.

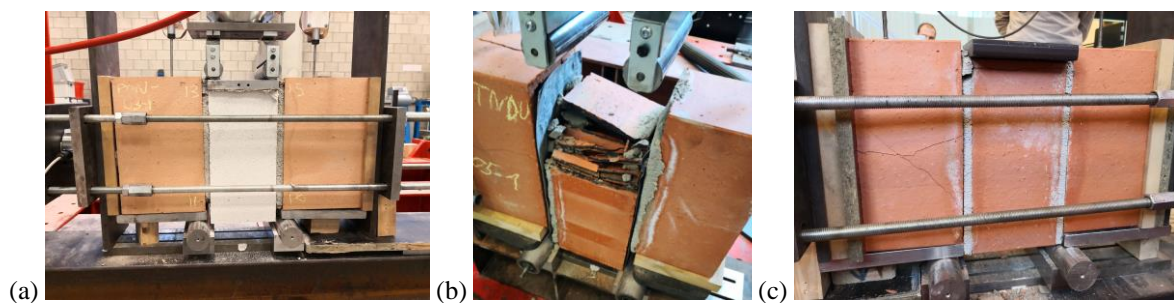


Figure 3. Examples of failure modes: (a) sliding of the joints, (b) crushing of the brick and (c) mixed failure of the brick obtained from different triplet tests [35].

Table 1. Material properties and dimensions of the masonry units.

Material	Dimensions ($l_u \times h_u \times t_u$) (mm)	Mean compressive strength (MPa)	Abbreviation
Perforated clay brick without tongue and groove	288 × 138 × 138	10.0	T
Perforated clay brick with tongue and groove	500 × 184 × 138	15.0	P
Autoclaved Aerated Concrete	600 × 150 × 140	4.5	A
General Purpose Mortar	-	5.0	N
Thin Layer Mortar	-	15.0	G

Table 2. Experimental results from the triplet tests.

Specimen name	Pre-compression level (MPa)			No. of tests per pre-compression level	Mean initial shear strength (MPa)	Mean friction coefficient	R^2
TTN	0.05	0.10	0.16	3	0.20	0.70	0.81
PPG	0.02	0.05	0.22	3	0.21	*	*
TAND	0.10	0.30	0.52	3	0.12	0.60	0.91
PAND	0.15	0.31	0.52	3	0.06	0.73	0.93

*Mohr–Coulomb curve could not be drawn due to a failure by combined crushing and sliding in PPG specimens

Table 3. Dimensions of the masonry wallettes tested under global in-plane shear loading.

Specimen name	Head joints	Wall dimensions ($l \times h \times t$)		
		l (mm)	h (mm)	t (mm)
TTN	Filled	1200	1200	138
PPG	Unfilled	1200	1074	140
TAND	Filled	1200	1135	138
PAND	Unfilled	1200	1111	140

2.2. Test set-up and instrumentation

Monotonic in-plane pushover tests were performed on twelve half-scale masonry panels, three for each type of specimen listed in Table 3. Three reference wall specimens, i.e. TTN1-3, were constructed with perforated clay bricks with GPM, and three were constructed with TLM, i.e. PPG1-3, to have a detailed understanding of the AAC and DPC's influence. Corresponding composite specimens were constructed, respectively TAND and PAND, where AAC blocks were placed at the bottom layer of the wall and the DPC layer was placed on top of it, in the middle of the mortar joint. Schematic diagrams of the different wallettes are shown in Fig. 4.

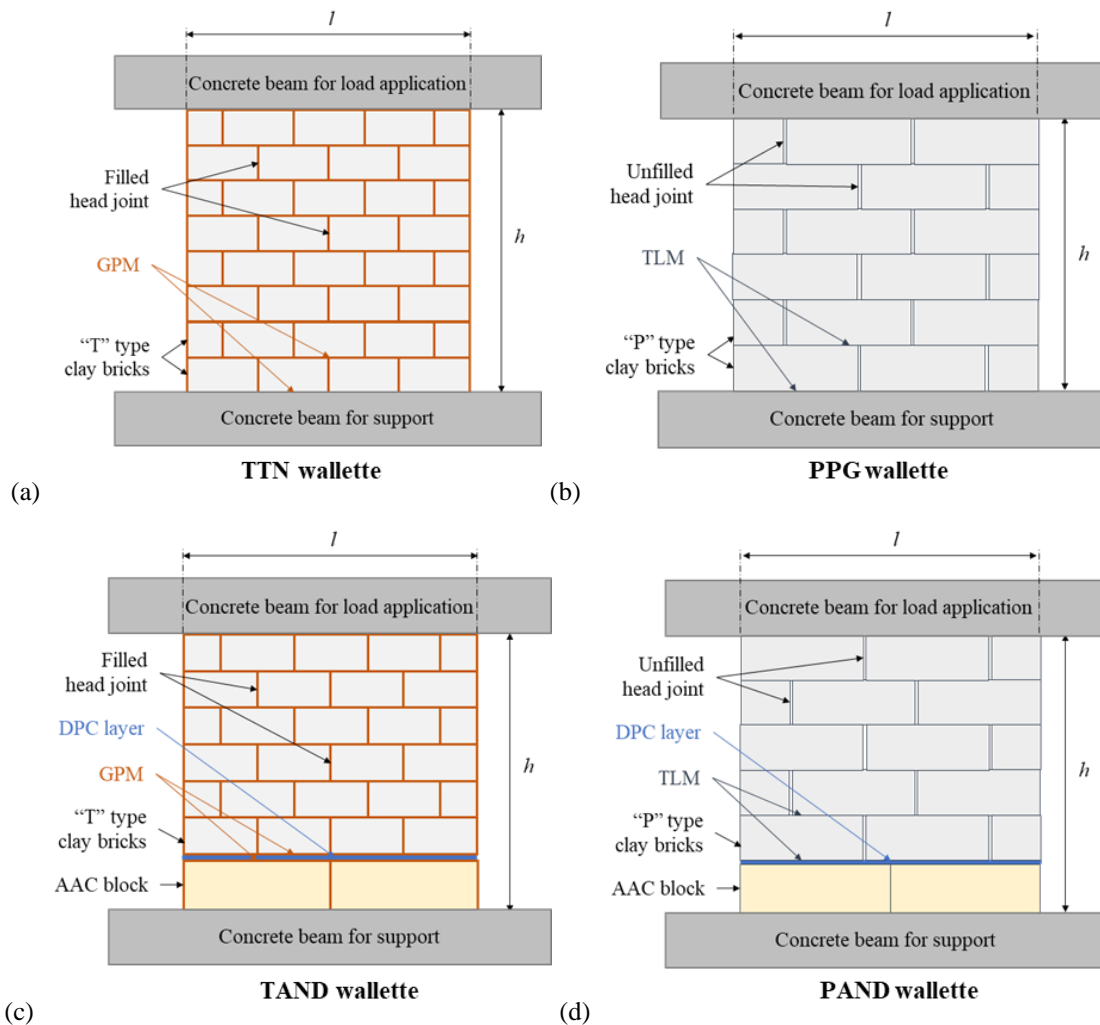


Figure 4. Schematic diagram (not to exact scale, dimensions given in Table 3) of the different wallettes tested under in-plane shear load: (a) TTN wallette, (b) PPG wallette, (c) TAND wallette, (d) PAND wallette.

As shown in Fig. 5a, the test set-up consists of several parts. A horizontal jack (1) was fixed with a thick steel plate to the reaction wall. A load cell (2) was placed on the jack, to measure the horizontal load applied to a concrete lintel on top of the wall specimen (5). A second prefabricated concrete lintel was fixed to the strong floor (7) with steel profiles and long bars (8). In the basement of the laboratory, two hydraulic jacks (10) with a load cell (9) on each of them were placed on a steel profile. This profile was connected with long bars (11) to the top of the wall specimen with another steel profile (3). The top profile spreads the pre-compression equally to the rollers (4) under it. The rollers were placed on a steel plate to reduce friction. The long steel bars of the wall panel (11) allow free horizontal movement at the top of the wall. LVDTs were placed at the back-face of the wall specimens (see Fig. 5b), whereas the front-face of the walls was used for DIC measurements (see Fig. 5c). The DIC captured the progress of the experiment with a refresh rate of 2 Hz. The LVDTs recorded at 10 Hz. Fig. 5b specifies the positions of all LVDTs. The global vertical displacement is measured on the top of the two ends of the concrete lintel, which are marked by numbers (1) and (2) in Fig. 5b.

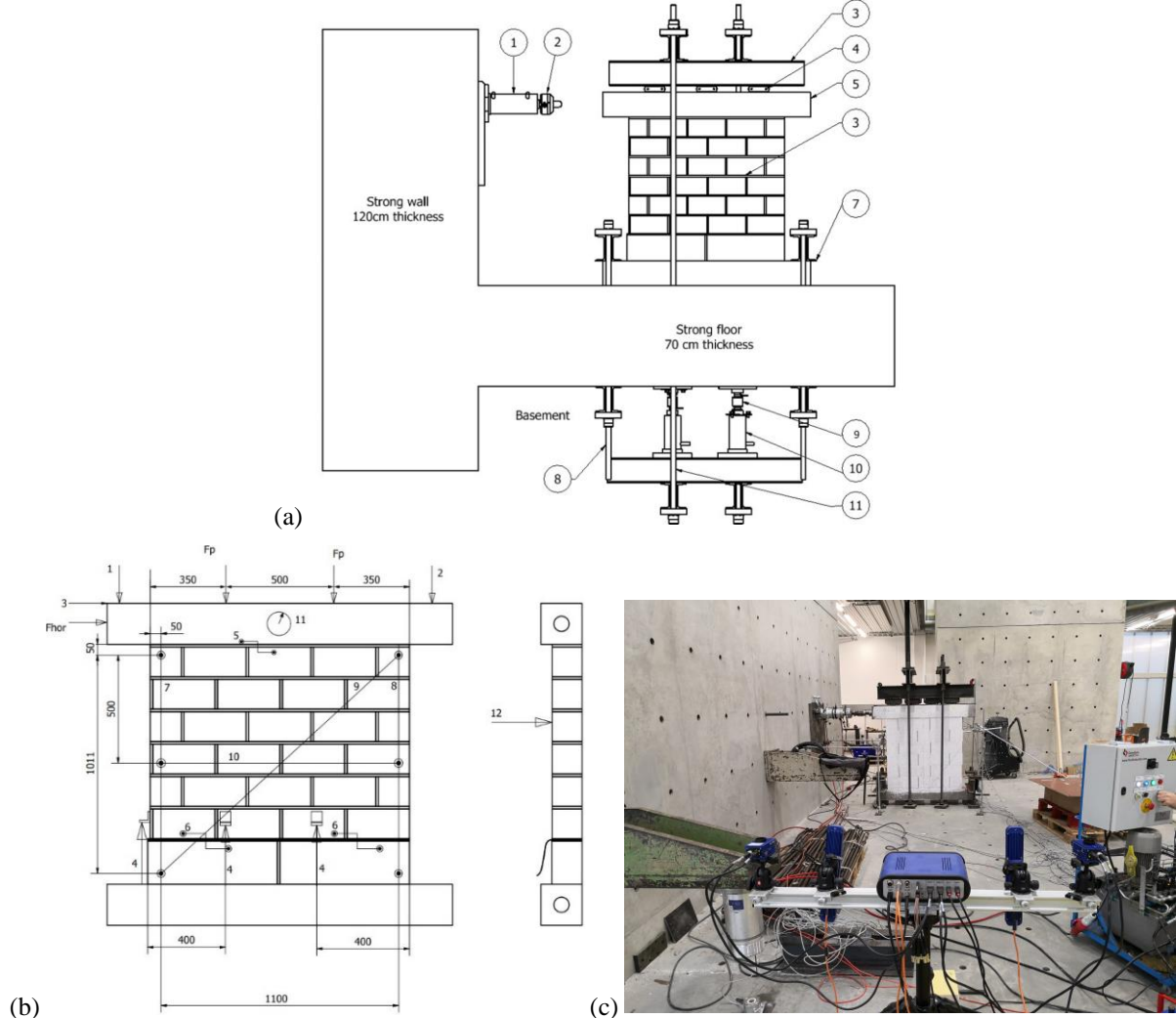


Figure 5. (a) Test set-up with a TAND wallette specimen in place (the different devices are numbered and explained in the text for better clarity), (b) positions of the LVDTs and inclinometer on a TAND specimen (all dimensions in mm) and (c) photograph of the test set-up with DIC (in foreground) and a PPG specimen (in background).

The combination of these two measurements could also calculate the global rotation of the masonry wall panel, yet an additional inclinometer was positioned in the middle of the top concrete lintel (11). The horizontal displacement corresponding to the applied shear load was measured next to the load cell (3). Slip of the top joint between the concrete lintel and the masonry bricks was measured by an LVDT (5). Wire-LVDTs were placed for the global deformation along the vertical axis (7, 8), horizontal axis (10) and diagonal (9). Uplift was measured in three places: at the beginning of the wall, at 1/3rd and 2/3rd of the wall's length. Uplift was measured from the concrete beam on the ground to the second layer of bricks for all experiments. Uplift was expected to be concentrated between the mortar and the DPC because of the limited adhesion between them. LVDTs (6) were also used to measure the slip between the first and second row of bricks. These were only placed for the specimens with an AAC-layer, thus measuring the possible sliding the level of the DPC. Global out-of-plane displacement was also measured using an LVDT (12).

3. Results and discussions

This section summarizes the relevant results in terms of load-displacement behaviour of the different wall specimens and their failure modes. Detailed comparisons are discussed between the reference configurations and the composite specimens with the AAC and DPC layers to characterize their influence on the performance of the wall. The experimental results are compared with available analytical models to get a detailed understanding about the in-plane shear resistance, predictability of the failure mechanisms and the initial stiffness of such composite masonry walls. Furthermore, the direct and indirect effect of the mortar type and the DPC layer is discussed.

3.1. Experimental force-displacement behaviour

In order to eliminate initial settlements, a small horizontal load and a vertical pre-compression load were applied on the wall specimens. A horizontal load of approximately 0.1 times the expected maximum horizontal load was applied first. Then the pre-compression load was increased from 0 to around 1.5 times the expected compression stress in service condition. A pre-compressive stress, $\sigma_0 = 0.5$ MPa, was applied and kept constant during the shear tests. Table 4 lists the constant values of pre-compressive stresses measured during each experiment. Finally, the horizontal load was applied until failure of the wall specimens. Fig. 6 compares the force-displacement behaviour of the TTN and TAND specimens and Fig. 7 compares the force-displacement behaviour of the PPG and PAND specimens obtained from the experimental campaign. The horizontal lines correspond to the ultimate analytical resistances ($V_{Rd,u}$) predicted by EN 1996-1-1 (discussed in Section 3.3) for the different specimens listed in Table 5. In general, a slight decrease of the maximum force can be noticed for all the specimens with the AAC and DPC layers, irrespective of the brick and mortar type. When the average values are compared between the relevant specimens with and without the thermal and damp-proof course layer (e.g. TTN vs TAND and PPG vs PAND), an approximately 8% (≈ 4 kN) strength reduction is noticed, confirming the fact that the AAC layer slightly weakens the masonry structure. The sudden drop of resistance in the PPG specimens is also noteworthy. This occurs due to the brittle nature of TLM and is discussed in the following section. A loss of stiffness can also be noticed for most of the specimens with the thermal and DPC layers (except TAND1 and PAND3). This occurs due to a horizontal sliding phenomenon between the first and the second layer of the wall specimens – where the DPC is placed (discussed in the following section). Therefore, based on the observed

experimental behaviour, it can be confirmed that the DPC influences the friction and consequently the sliding shear resistance of the walls, while the AAC influences the compressive strength, which affects the diagonal shear resistance as well as the flexural resistance of the masonry walls. Table 4 lists the experimental outcomes for all specimens in terms of the applied (constant) pre-compressive stresses (σ_0), peak in-plane shear resistance (V_{exp}), initial stiffness (K_0 , obtained with a tangent from the experimental load-displacement curves) and the failure modes obtained from the experiments.

No tests on a similar shape and initial compression level have been identified in the literature and a direct comparison of the composite walls made of only AAC units is therefore not possible at this stage. However, comparing the load-displacement curves presented in [20] and [39] on different configurations of AAC walls or on AAC wallettes loaded in diagonal compression, it appears that the post-peak behaviour of the composite specimens is very similar in shape, with a rather long stable plateau and eventually some softening, opposite to the sharp resistance drop observed for pure clay specimens. This confirms that the global behaviour of the composite specimens is mainly governed by the weaker AAC layer.

Table 4. Experimental results and failure modes.

Specimens	Pre-comp. force, N_{Ed} (kN)	Pre-comp. stress, σ_0 (MPa)	Peak exp. shear resistance, V_{exp} (kN)	Initial stiffness, K_0 (N/mm)	Experimental failure
TTN1	82.78	0.4999	43.4	8979	Diagonal shear sliding + Toe crushing
TTN2	82.89	0.5005	39.9	5662	
TTN3	82.92	0.5007	40.5	17612	
TTN (avg)	82.86	0.5004	41.3	10751	
TAND1	83.26	0.4956	36.6	8591	Horizontal shear sliding + Toe crushing
TAND2	83.27	0.4957	36.9	8907	
TAND3	82.76	0.4926	40.0	12901	
TAND (avg)	83.10	0.4946	37.8	10133	
PPG1	82.91	0.4935	44.0	12427	Diagonal shear sliding + Toe crushing
PPG2	82.84	0.4931	42.7	11853	
PPG3	82.89	0.4934	39.0	11714	
PPG (avg)	82.88	0.4933	41.9	11998	
PAND1	83.18	0.5023	39.9	7870	Horizontal shear sliding + Toe crushing
PAND2	82.75	0.4997	37.7	6537	
PAND3	82.82	0.5001	40.3	14038	
PAND (avg)	82.92	0.5007	39.3	9482	

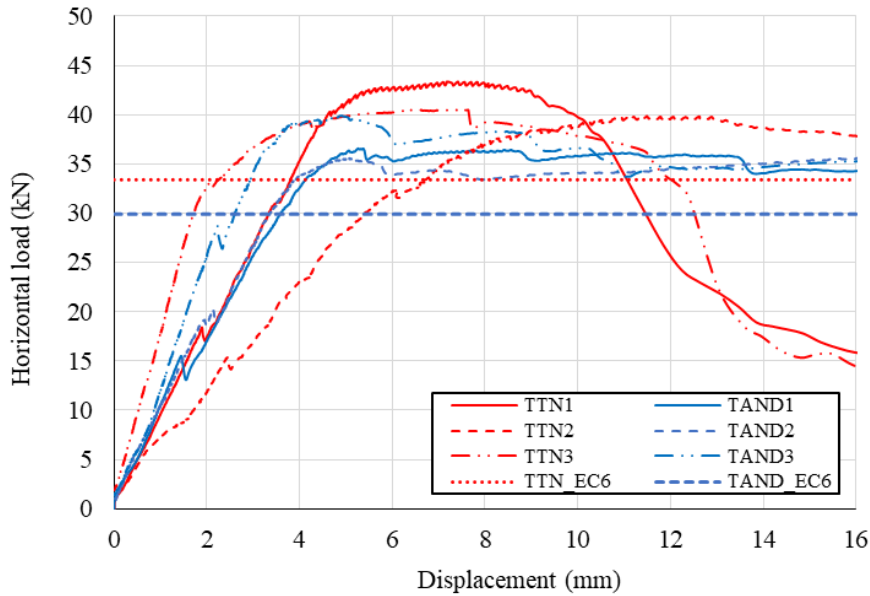


Figure 6. Load-displacement diagram for TTN and TAND specimens.

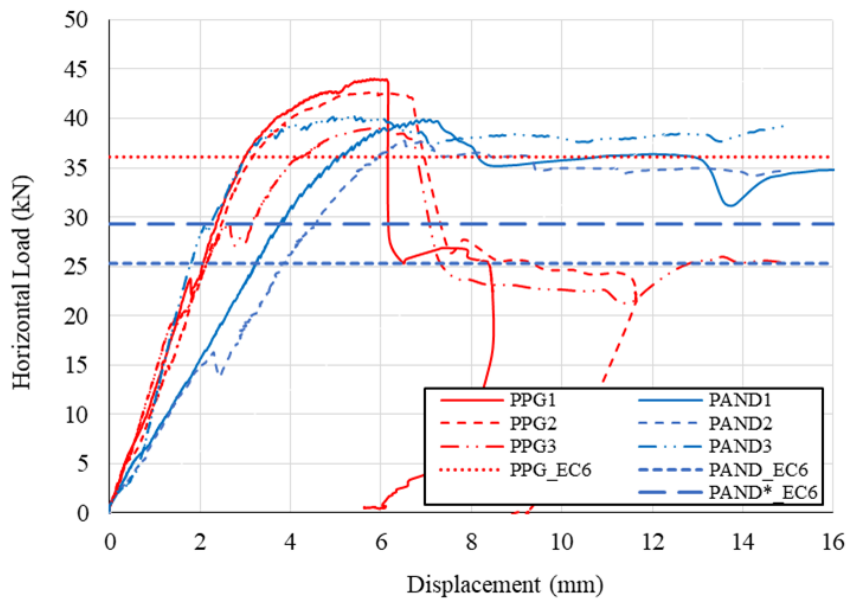


Figure 7. Load-displacement diagram for PPG and PAND specimens.

3.2 Observed failure modes

The typical failure patterns observed in masonry structures subjected to a combination of vertical and in-plane horizontal loading are (i) flexural failure and (ii) shear failure. The flexural failure is generally visualized by an uplifting phenomenon (i) without toe crushing (TC) – the wall acts as a rigid body and offers a pure rocking behaviour (Fig. 8a) or (ii) with toe crushing (Fig. 8b). Similarly, the shear failure generally occurs due to two reasons: (i) diagonal shear cracking (Fig. 8c) and (ii) shear sliding (SS). Two types of shear sliding can be noticed in masonry walls: (i) horizontal shear sliding (Fig. 8d), and (ii) diagonal shear sliding (Fig. 8e). As this paper focuses only on the in-plane behaviour of masonry walls, out of plane failure modes are not discussed in this study.

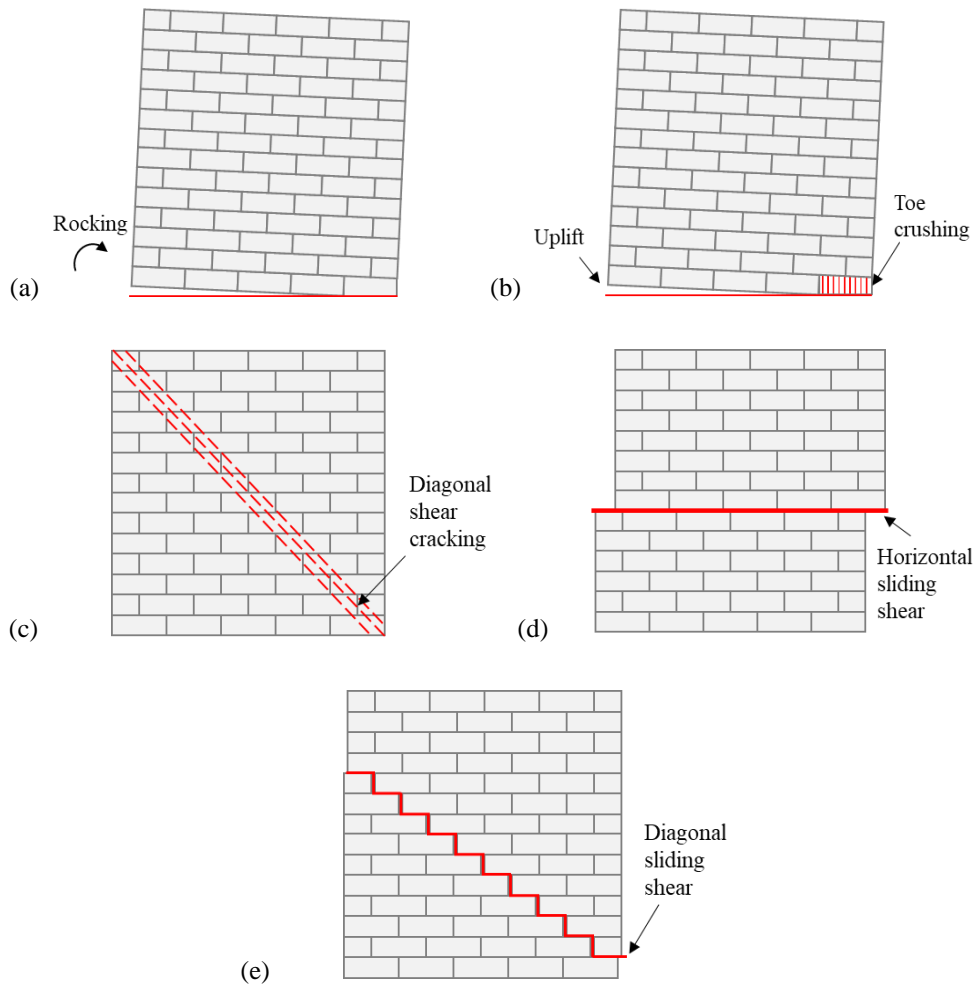


Figure 8. Failure patterns in URM masonry walls under in-plane lateral load: (a) pure rocking; (b) uplift with toe crushing (TC); (c) diagonal shear cracking; (d) horizontal shear sliding (HSS) and (e) diagonal shear sliding (DSS).

An uplift was clearly visible for all the tested wall specimens when the horizontal load was increased. However, different failure mechanisms were noticed for the different specimens. The six reference walls (TTN and PPG specimens) failed due to a combination of diagonal shear sliding through the joints and toe crushing of the wall. On the other hand, the six specimens with the AAC and the DPC layer (TAND and PAND) showcased a significant horizontal shear sliding at the DPC layer, ultimately leading to a toe crushing of the AAC unit. The progressive evolution of axial and shear strains at various stages of each test was captured by the DIC apparatus. Some examples regarding the four different types of specimens (TTN, TAND, PPG and PAND) are presented in Fig. 9-16 with respect to different points marked in their corresponding load-displacement curves. Each figure essentially highlights the evolution of the axial and shear strains through the wall specimen, where the maximum positive and negative strain values are respectively represented by the colour red and blue. The vertical black zones in the DIC images are due to the shadow of the vertical bars of the load introduction system (as visible in Figures 5 and 17). The gradual uplift in all the specimens is clearly visible from the evolution of the axial strains shown in Fig. 9, 11, 13 and 15. The reference walls with GPM (e.g. TTN1) experienced an uplift up to $2/3^{\text{rd}}$ of the width of the wall (see Fig. 9). A similar uplift behaviour is noticed for the reference walls with TLM (e.g. PPG2) as shown in Fig. 11. On the other hand, the specimens with an AAC and DPC layer (e.g. TAND2 and PAND1) are observed to exhibit uplifts in two horizontal joints, leading to a different failure progression. Initially, at a lower level of

lateral load, an uplift takes place at the base of the wall specimens between the AAC layer and the bottom concrete lintel (see Fig. 11b-c and Fig. 15b-c). This uplift progresses along half of the wall length. Then, at a higher level of lateral load, uplift is noticed between the first and the second layer of the wall specimens where the DPC was placed (see Fig. 11d-e and Fig. 15d-e). This uplift was larger and occurred along $2/3^{\text{rd}}$ of the wall length.

The development of the uplift phenomenon directly influences the shear strain evolution through the wall specimens as shown in Fig. 10, 12, 14 and 16 for the different specimens. Initially, high shear strains develop at the toe end of the TTN wall specimens with a $1/3^{\text{rd}}$ wall uplift (see Fig. 9c and 10c). Then, with increasing lateral load and subsequent uplift of the wall, stresses get redistributed to the wall section and diagonal staircase-type shear strains develop through the TTN specimens (from bottom right corner to top left corner) as shown in Fig. 10d-e. Finally, at approximately $2/3^{\text{rd}}$ wall uplift, stresses can no longer redistribute and complete failure occurs (see Fig. 9f and 10f) due to a combination of diagonal sliding and toe crushing. A similar failure progression can be noticed for the PPG specimens, but with a significant qualitative difference. In these specimens, the initial shear strains at the toe end of the wall were quite localised compared to the TTN specimens (see Fig. 14c). With an increase in the horizontal load and consequently the uplift of the wall, the diagonal staircase-type shear strains evolved in an abrupt and sudden manner through the wall specimen, resulting in an instant loss of resistance in the PPG specimens (i.e. sudden drop in Fig. 7). This occurs due to the brittle nature of TLM, which was also noticed during the triplet tests [35], done prior to this study. The TAND and PAND specimens showcased a different progression. Initially, during the uplift at the bottom of the wall specimens, shear strains develop at the toe end of the walls. Then, with increasing lateral load, both the axial and shear strains develop between the first and the second layer of the wall specimens – where the DPC is placed. However, once the peak load is reached, the shear strains remain constant while the uplift (axial strains) increases, leading to a toe crushing of the AAC unit. Horizontal shear sliding is noticed at the DPC layer till the end of the experiments. A slightly higher resistance was obtained from the specimens with a TLM than the ones with a GPM, due to the fact that, the compressive strength of the individual masonry units with TLM is higher and the clay bricks acted more as a rigid body. Fig. 17 showcases the ultimate state of one of the tested wall specimens corresponding to each configuration.

The behaviour observed for the classical full-clay homogenous wall specimens is well-known and has already been reported by other authors [33]. Such a behaviour is characterized by a rather brittle behaviour of the typical hollow clay units used in many countries in North-Western Europe, in particular when assembled with thin-layer glue mortar. On the contrary, the behaviour of the composite specimens is essentially different due to (i) a lower tension resistance (adhesion) between the DPC and the other materials, triggering an anticipated opening of the horizontal joint in the tension zone of the wall at two levels, i.e. at the AAC-foundation interface, similar to what is commonly observed at the base of walls, but also at the AAC-DPC interface; (ii) reduced friction properties in presence of DPC, as reported from the triplet tests in section 2, accelerating the sliding of the clay part with respect to the DPC/AAC part; and (iii) a lower compression resistance, yet less brittle, of the AAC, although this effect is not as relevant as in the homogenous walls, where a significant drop in resistance is observed due to the toe crushing of the corner unit, while the behaviour of the composite elements is only characterized by a very limited drop in resistance (from point B to point C in the TAND and PAND specimens), allowing the specimens to keep its resistance while the upper part is sliding with respect to the lower one.

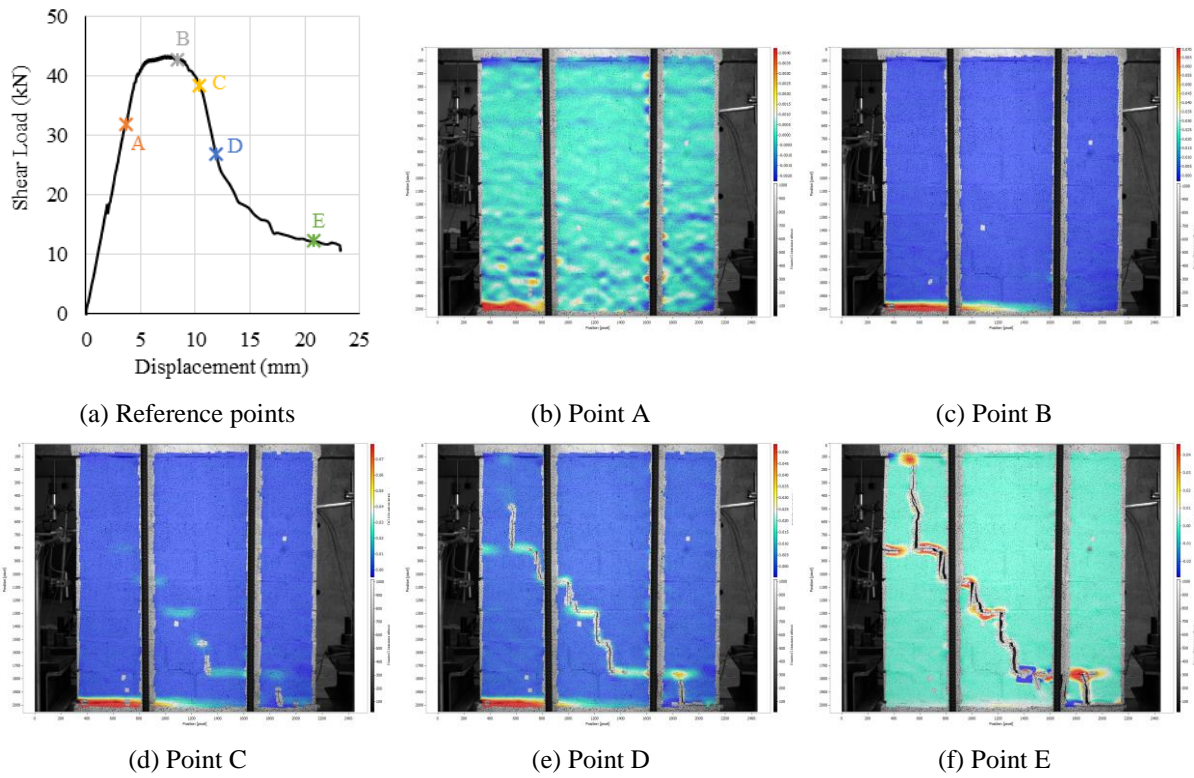


Figure 9. Progression of axial strains TTN1.

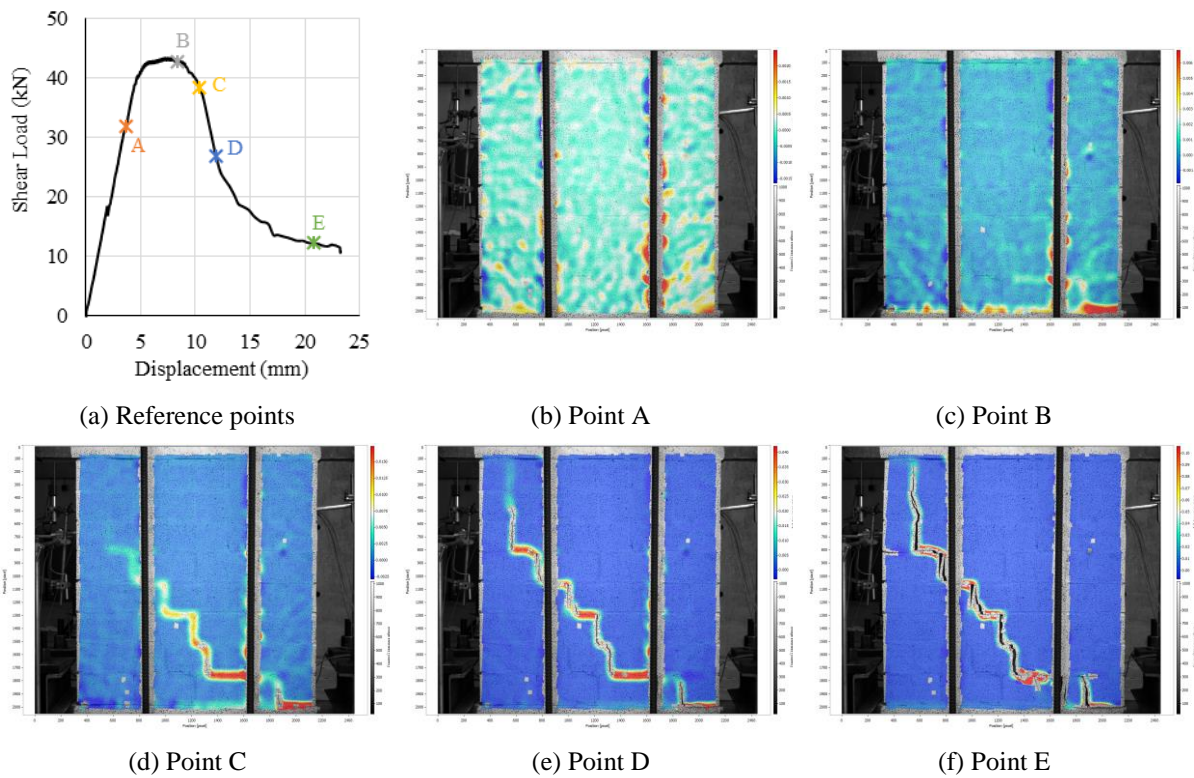


Figure 10. Progression of shear strains TTN1.

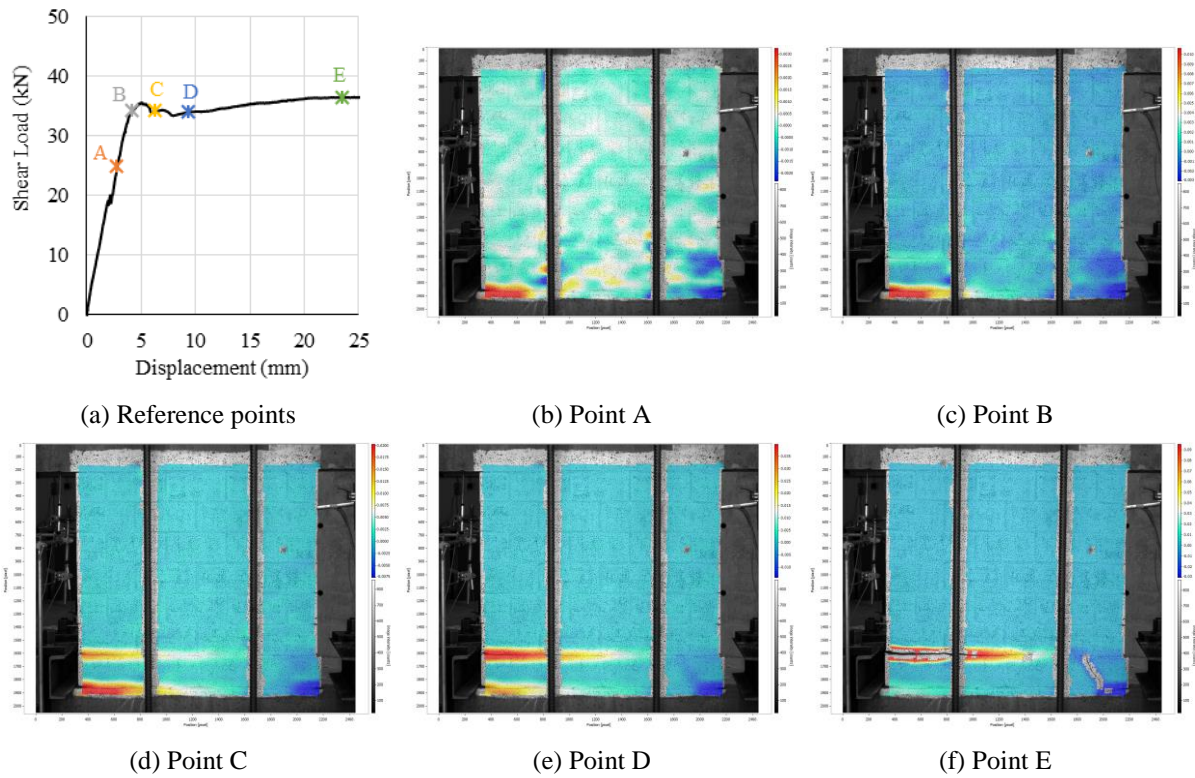


Figure 11. Progression of axial strains TAND2.

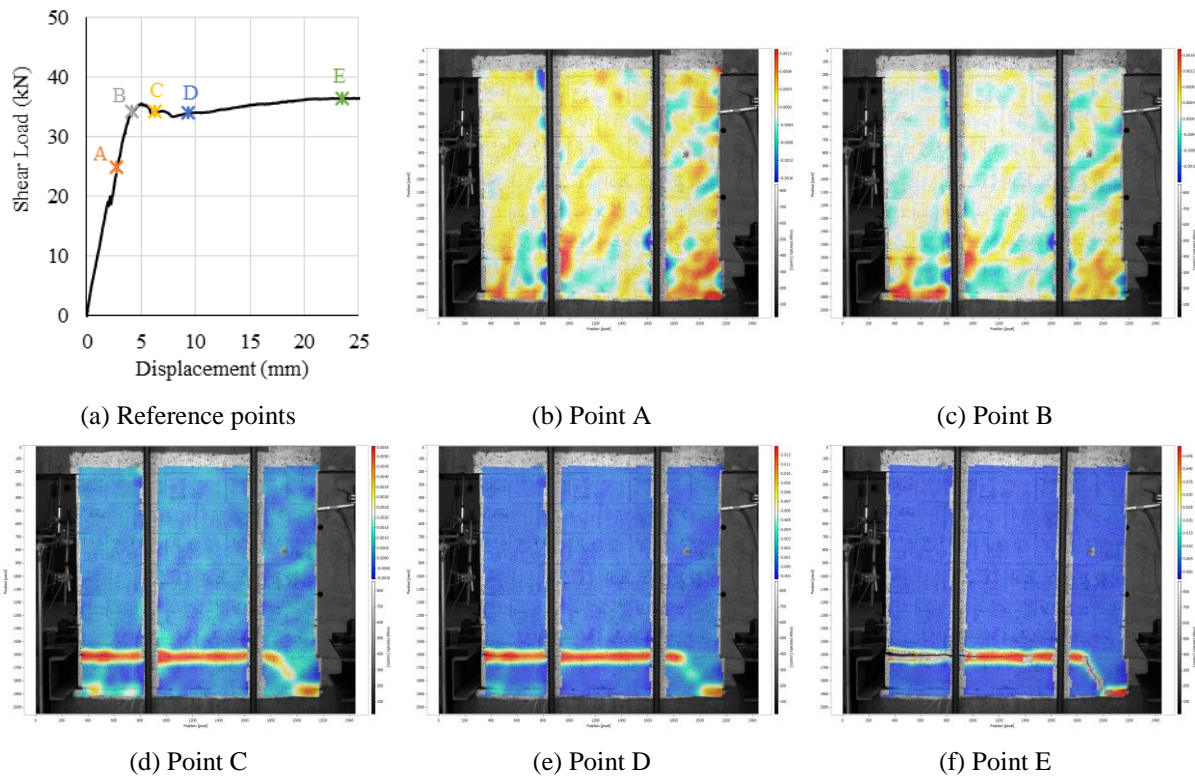


Figure 12. Progression of shear strains TAND2.

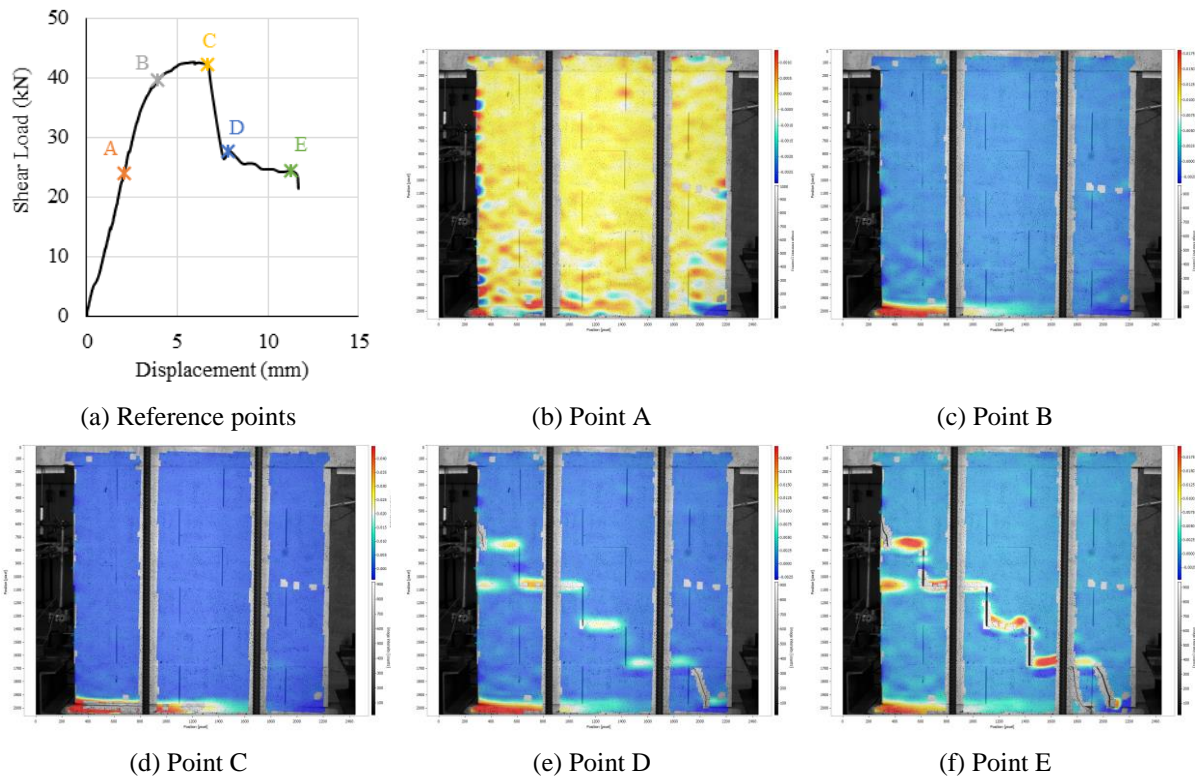


Figure 13. Progression of axial strains PPG2.

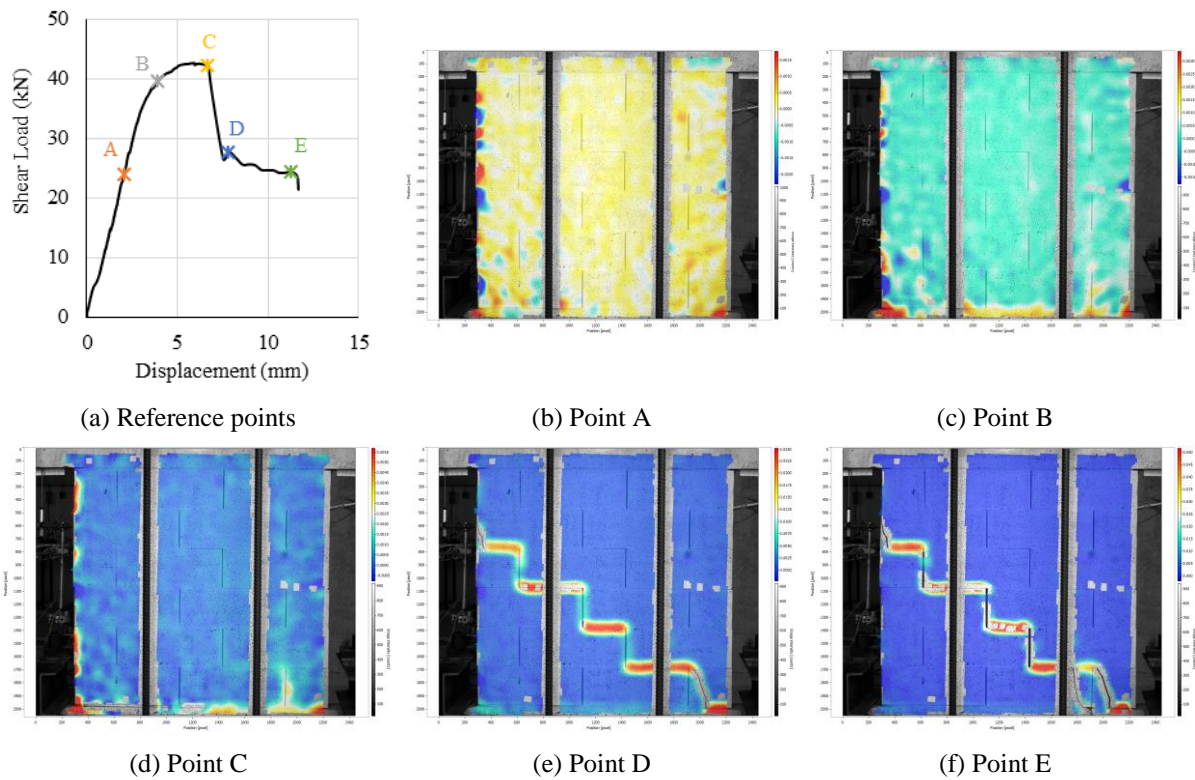


Figure 14. Progression of shear strains PPG2.

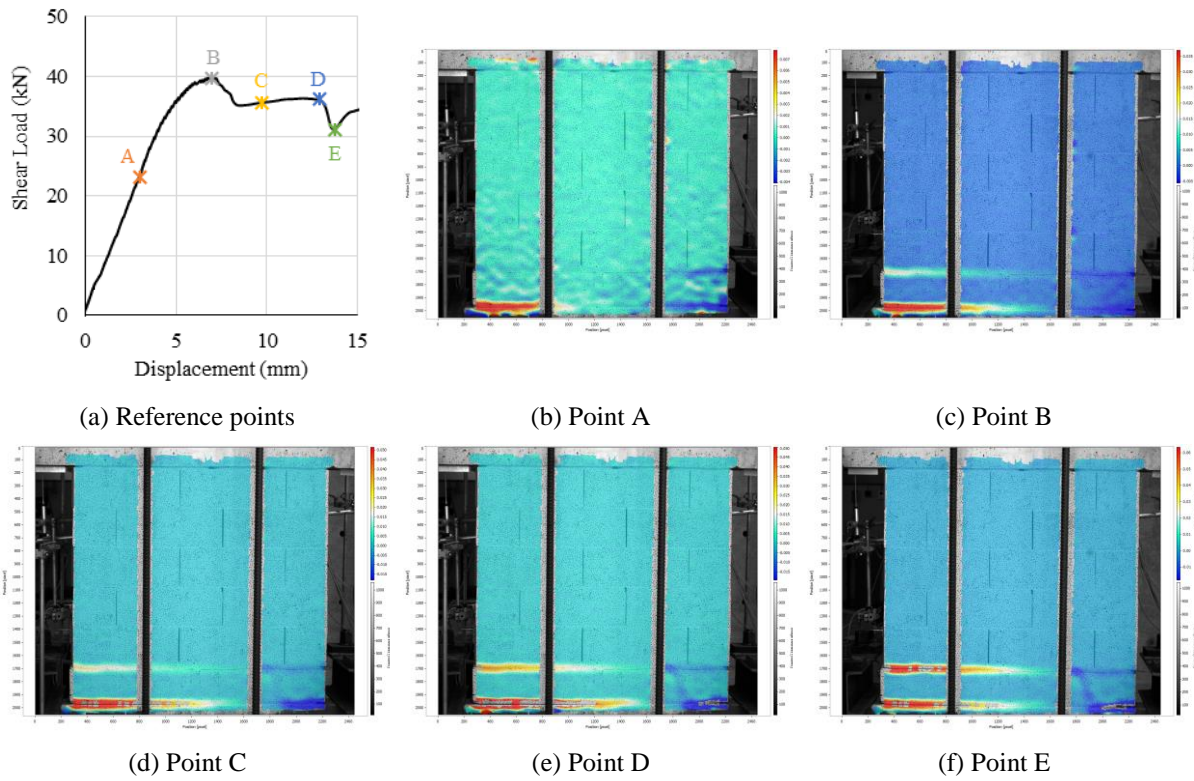


Figure 15. Progression of axial strains PAND1.

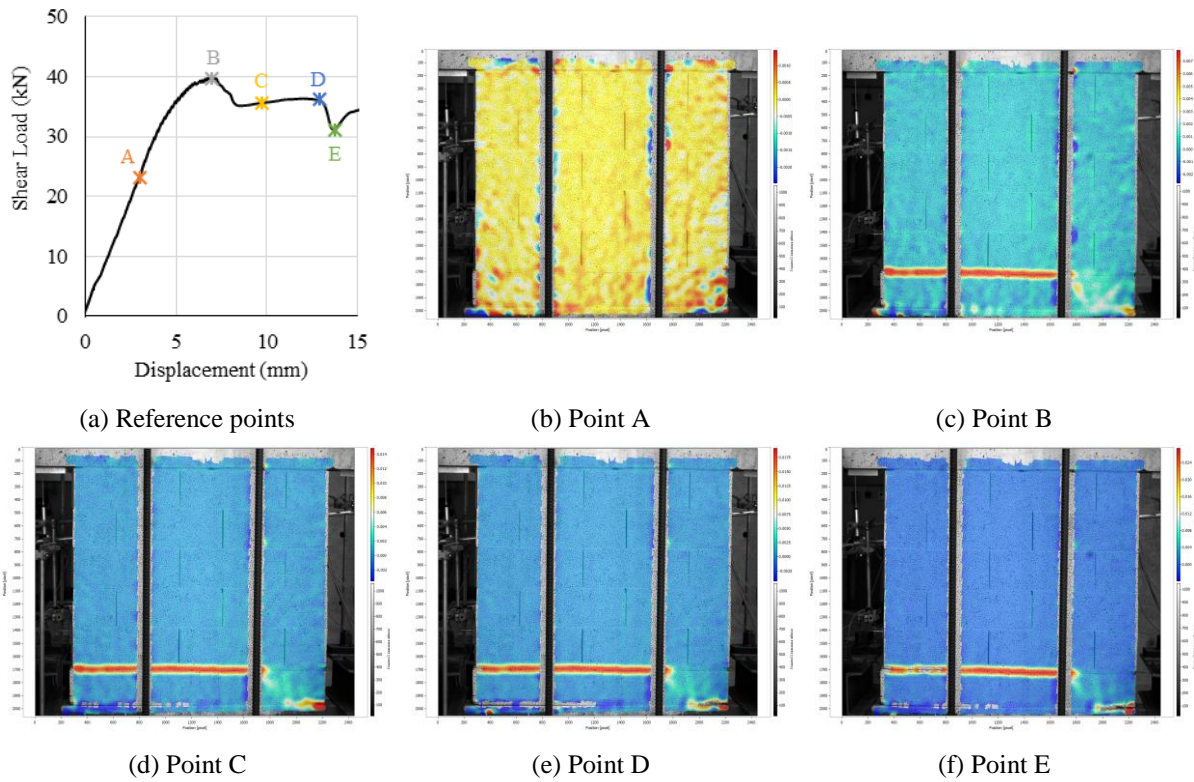


Figure 16. Progression of shear strains PAND1.



Figure 17. Ultimate failure modes of the wallettes: (a) TTN1 – Diagonal shear sliding (DSS) with toe crushing (TC), (b) TAND2 – Horizontal shear sliding (HSS) with toe crushing (TC), (c) PPG2 – Diagonal shear sliding (DSS) with toe crushing (TC) and (d) PAND3 – Horizontal shear sliding (HSS) with toe crushing (TC).

3.3 Analytical assessment of the specimens according to EN 1996-1-1 [5]

Standard analytical methods are recommended by EN 1996-1-1 [5] to predict the in-plane shear resistance of conventional masonry structures. However, the analytical relationships do not explicitly include the composite aspect, i.e. when the masonry structure is built up with different types of elements (masonry units, mortar, AAC, DPC etc.), under in-plane shear loads and therefore needs further validations. To that purpose, a detailed

assessment was conducted on the following analytical method with respect to the experimental results. Relevant analytical values are listed in Table 5 along with the failure modes predicted by EN 1996-1-1.

According to Clause 8.3.1 of EN 1996-1-1 [5], the shear resistance (V_{Rd}) of an URM wall subjected to a combination of vertical and horizontal in-plane loading can be calculated as:

$$V_{Rd} = f_{vd} \cdot t \cdot l_c \quad (1)$$

Where, f_{vd} is the design shear strength of masonry and can be obtained by dividing the characteristic shear strength of masonry, f_{vk} , by the relevant partial factor for materials, γ_M , t is the thickness of the wall, and l_c is the length of the compressed part of the wall. Although, l_c according to EN 1996-1-1 is determined based on a linear stress distribution (see Fig. 18), some other variations have been investigated and are discussed in section 3.3.2. However, all safety factors are considered to be 1.0 while comparing the analytical results with the experimental outcomes in the following sections and therefore characteristic values are used instead of the design values. To that purpose, f_{vk} can be calculated according to clause 5.7.2 of EN 1996-1-1 for filled and unfilled head joints as shown in the following equations.

For filled head joints:

$$f_{vk} = f_{vk0} + \mu_f \sigma_d \leq f_{vlt} = 0.065 f_b \quad (2)$$

For unfilled head joints:

$$f_{vk} = 0.5 f_{vk0} + \mu_f \sigma_d \leq f_{vlt} = 0.045 f_b \quad (3)$$

Where, f_{vk0} is the characteristic initial shear strength under zero compressive stress, μ_f is the characteristic friction coefficient, σ_d is the average compressive stress acting on the compressed part of the wall specimen. Mean values obtained from the abovementioned triplet tests are considered for f_{v0} instead of the characteristic values to have a direct comparison with the experimental outcomes. μ_f is considered equal to 0.4 as per EN 1996-1-1. Experimental values from [35] were not considered in this aspect due to a high coefficient of variation ($\approx 7.8\%$). Moreover, $\mu_f = 0.4$, being a lower bound compared to the experimental values, offers a safe analytical estimation. f_{vlt} denotes a limiting value of f_{vk} , and corresponds to the compression in the diagonal struts created after the occurrence of the diagonal shear cracks shown in Fig. 8c. For the application of the EN 1996-1-1 procedure to composite walls, it is considered that f_b is the normalized compressive strength of the weakest masonry unit in the wall (e.g. AAC for the TAND and PAND specimens) and can be obtained from the mean or declared compressive strength of the masonry units with relevant shape factors defined in EN 772-1 [3] or the relevant national annexes. On the other hand, the general equation of f_{vk} corresponds to the shear sliding failure mechanism. A distinct characterization between the horizontal and diagonal shear sliding is however not provided by the EN 1996-1-1.

The design in-plane shear resistance, V_{Rd} , corresponding to the load case considered in the experiments can be calculated according to Fig. 18, where a horizontal force is applied at the top of a cantilever wall (shear span ratio = 1), h is the height and l is the length of the wall, R_{Ed} denotes the reaction force acting on the compressed part of the wall, l_c . The eccentricity between the central axis of the wall and the axis of the reaction force is denoted by e . The horizontal force or design shear load (V_{Ed}) can increase to a maximum value until the design shear resistance (V_{Rd}) is reached or the length of the compressed part becomes zero (i.e. the wall will tip over and rotate). Moreover, EN 1996-1-1 recommends a verification at the base of the wall to account for a possible toe crushing phenomenon. The flexural resistance of a rectangular wall section can be calculated for a given compressive force assuming a rectangular stress block as per clause 8.3.2.5, EN 1996-1-1.

$$M_{Rd} = \frac{N_{Ed} \cdot l}{2} \left(1 - \frac{N_{Ed}}{t \cdot l \cdot \eta_f \cdot \Phi \cdot f_d} \right) \quad (4)$$

Where N_{Ed} is the vertical load applied on top of the wall, l is the total length of the wall, t is the thickness of the wall, f_d is the design compressive strength of masonry, Φ is the reduction factor according to clause 8.3.2(2) and η_f is the factor defining the equivalent rectangular stress block. The characteristic compressive strength of masonry, f_k , has been calculated according to clause 5.7.1.4 of EN 1996-1-1 and is used with a γ_M factor equal to 1.0 to have a direct comparison with the test results. As the masonry units were produced by a Belgian company, the K value required to determine f_k is taken from EN 1996-1-1 ANB [38]. As for the shear resistance, the procedure is applied considering the resistance of the bottom layer of the wall, being also the weakest.

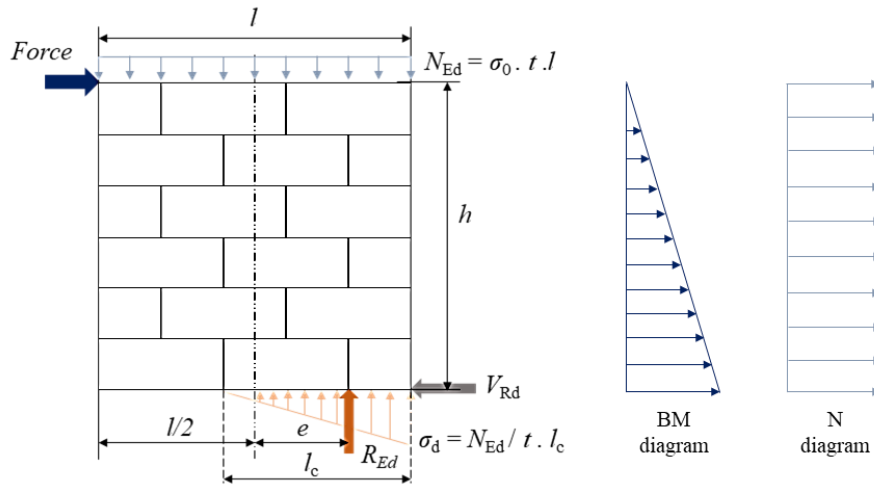


Figure 18. Force transfer mechanism of a masonry wall under combined vertical and horizontal loading.

The in-plane shear resistance, V_{Rd} , of a masonry wall is considered to be the minimum value between: (i) sliding shear failure ($V_{Rd,s1}$ in Table 5, corresponding to f_{v0}) and (ii) diagonal shear failure ($V_{Rd,s2}$ in Table 5, corresponding to f_{vt}). Relevant factors were considered for filled and unfilled head joints. The flexural resistance, M_{Rd} , of the masonry walls were also calculated as per Eq. 4. The η_f factor was considered as 0.85 for this study. The Φ factor corresponds to any possible eccentricities related to the vertical load application. Although EN 1996-1-1 recommends a 0.9 value for Φ to account for the eccentricities in real-life design of masonry walls, the test set-up and load application discussed in this study were built with utmost care in order to avoid any eccentricities related to the vertical load. Therefore, the Φ was considered as 1.0 to have a consistent comparison between the experimental results and the analytical calculations listed in Table 5. The maximum allowable horizontal force $V_{Rd,f}$ corresponding to reaching M_{Rd} with a shear span ratio equal to 1.0 is calculated and compared with $V_{Rd,s1}$ and $V_{Rd,s2}$ to obtain the ultimate horizontal resistance of the specimens, $V_{Rd,u}$. $V_{Rd,u}$ is defined as the minimum value among $V_{Rd,s1}$, $V_{Rd,s2}$ and $V_{Rd,f}$ and is subsequently compared with the experimental force-displacement curves in Fig. 6-7 (denoted by _EC6). In Table 5, $V_{exp,avg}$ denotes the average values of the peak shear strength, H_{max} (see Table 4), obtained from the tests on each type of masonry specimens.

3.3.1 Ultimate in-plane lateral resistance and failure patterns

A decent and conservative agreement is found between the analytical and experimental values corresponding to the reference specimens with a single type of masonry unit, i.e. TTN and PPG. The experimental

resistance was found to be 1.15-1.23 times larger than the analytically predicted values, signifying a realistic safety margin (see Fig. 6-7 and Table 5). The different types of clay bricks used in the TTN and PPG specimens did not have any qualitative impact on the results. However, some quantitative differences were noticed between TTN and PPG from both the analytical and experimental results, as the PPG specimens offered a higher lateral resistance compared to the TTN specimens. This occurred because the “P” type perforated clay bricks with tongue and groove had a larger compressive strength (15 MPa) than the “T” type clay bricks without tongue and groove (10 MPa).

A good agreement can also be noticed between the analytical and experimental outcomes for the specimens with AAC and DPC layers and filled head joints, i.e. TAND. Furthermore, a comparison between the experimental and analytical results concerning the TTN and the TAND specimens highlighted the fact that the in-plane lateral resistance of the masonry walls reduces in the presence of an AAC layer due to the lower compressive strength of this layer. However, the analytical predictions corresponding to the PAND specimens proved to be quite conservative. While the experimental outcomes showed a slightly better resistance for the PAND specimens compared to the TAND specimens (as anticipated due to the higher compressive strength of the “P” type clay bricks), the analytical calculations predicted the opposite. The possible reason behind such a prediction can be the fact that, although the vertical head joints between the clay bricks were unfilled in these specimens, the vertical head joints between the AAC units at the bottom layer were filled. So, the joints can neither be defined as filled nor unfilled and therefore, cannot be categorized according to EN 1996-1-1, which only offers a straightforward characterization for each specific type of head joints, i.e. filled or unfilled. When the head joints in the PAND specimens are considered to be unfilled, the EN 1996-1-1 recommends a limit of $0.045f_b$ to calculate the diagonal shear resistance of the wall specimens and at the same time, states that the weakest material (AAC in this case) should be considered to calculate f_b . Furthermore, an additional reduction factor of 0.5 is provisioned in regards to the mean initial shear strength (f_{vk0}) to estimate the sliding shear resistance of the walls. This pushes towards an absolute worst-case scenario and as a result, underestimates the overall shear strength of the wall specimens. On the contrary, the experimental behaviour of the wall specimens was observed to be governed by the bottom layer of the wall made of AAC units with filled head joints. Therefore, it is deemed more reasonable to estimate the in-plane shear strength of the PAND wall specimens considering filled head joints. To that purpose, an additional set of calculations has been made as shown in Table 5, where filled head joints are considered for the PAND specimens (denoted as PAND*) and essentially leads to a more realistic prediction.

A combined failure (resistance values with close margins) due to flexure and shear is predicted by EN 1996-1-1 for the reference configurations, TTN and PPG, whereas a shear failure in the form of diagonal shear cracking is predicted for the specimens with an AAC and a DPC layer, i.e. TAND and PAND. Similar failure modes were obtained during the experiments as all the test specimens failed due to toe crushing, which occurred either by reaching the diagonal shear capacity or the flexural capacity of the wall specimens. Significant shear sliding was also noticed in the specimens prior to the ultimate failure.

3.3.2 Influence of the stress distribution along the compressed part of the wall

Axial strains in the vertical direction were extracted from the DIC apparatus to analyze the compressed length, l_c , at the bottom of the wall (i.e. the critical zone) and compare it with the analytical prediction. The axial strain values are plotted in Fig. 19 with respect to the length of the wall (load-application side of the wall = 0 mm), for the aforementioned points (i.e. A, B, C, D) marked in the load-displacement curves shown in Fig. 9-16. Point

E is not used as it corresponds to a severely damaged post-failure state of the wall specimens. The graphical data is shown for the one specimen per typology (i.e. the same specimens used earlier for strain visualization in Figures 9-16, TTN1, TAND2, PPG2 and PAND1). Similar results were obtained for the other specimens. It can be clearly seen that, for all the specimens, the axial strains remain quite low at the initial stages of the horizontal load application (Point A), hinting towards a negligible uplift. As a result, almost 50% of the wall length stays in contact. As the load increases and the specimens reach their maximum capacity (Point B), a significant uplift is noticed. l_c reduces to a range of 300-350 mm at this stage and remains approximately constant for later stages as well, i.e. Point C and D.

As stated earlier, the EN 1996-1-1 analytical model to calculate the design shear resistance of a masonry wall is based on a linear stress distribution at the bottom of the wall along l_c (see Fig. 18). This is denoted as l_{c_linear} in Table 5. On the contrary, a rectangular stress block or a uniform stress distribution is suggested to verify against flexure by EN 1996-1-1, clause 8.3.2.5. Therefore, in order to have a consistent comparison between the experimental and analytical values of the compressed length, further calculations have been carried out assuming a uniform stress distribution along the compressed length of the wall i.e. $l_{c_uniform} = 2 \left(\frac{l}{2} - e \right)$. The calculated values for $V_{Rd,s1}$, $V_{Rd,s2}$ and $l_{c_uniform}$ are listed in Table 6. It can be noted that some models are suggesting a parabolic distribution. Results obtained with such an alternative version are likely to fall between the boundaries given by the linear and the uniform models. This option is therefore not considered further in this paper, but could be considered in a future refined analysis.

Another aspect has also been deemed noteworthy during the experiments. The uplift at the base of the wall specimens with an AAC layer was sometimes observed to be discrete, i.e. individual masonry units lift up as a whole rather than according to a gradient-like elevation. So, a different set of calculations has been carried out to compare the discrete values of the compressed length and the resulting V_{Rd} values with the experimental results as shown in Table 7. The discrete values are calculated as, $l_{c_discrete} = \min(l_{c_linear}, l_u)$, where l_u denotes the length of a masonry unit and l_{c_linear} denotes the compressed length calculated considering a linear distribution of stresses. All three different analytical values of the compressed length, obtained for the different specimens, are compared with the axial strains obtained at Point B, which approximately corresponds to an ultimate limit state of the wall specimens. The analytical values of the compressed length are denoted by the vertical lines in Fig. 19 and are plotted with respect to the compressed side of the wall.

Based on the comparison studies, it can be stated that the Eurocode procedure provides a good estimation of the compressed length for the reference configurations, TTN and PPG. The $l_{c_uniform}$ and $l_{c_discrete}$ values prove to be rather conservative. However, the Eurocode procedure overestimates the compressed length for the wall specimens with an AAC layer (TAND and PAND). The $l_{c_uniform}$ and $l_{c_discrete}$ values prove to be more realistic when compared to the experimental axial strain values as well as the visible uplifts noticed during the tests. But, the resulting resistances corresponding to $l_{c_uniform}$ and $l_{c_discrete}$ (see Table 6 and 7 respectively) are noticed to be quite conservative and therefore cannot be stated as an optimal design consideration. Finally, the highly overestimated value of l_{c_linear} calculated for the PAND specimens can be stated as unrealistic and further justifies the fact that using the reduction factors for unfilled head joints might not be the optimal way to characterize such composite masonry walls. The analytical values obtained for the PAND specimens assuming filled joints and a linear stress distribution at the compressed part i.e. $V_{Rd,u} = 29.33$ kN and $l_{c_linear} = 639.4$ mm, provides a more realistic behaviour.

Table 5. Analytical results according to EN 1996-1-1 assuming $l_{c,linear} = 3 \left(\frac{l}{2} - e \right)$

Specimens	Experimental values			Sliding shear (SS)						Diagonal shear (DS)			Flexural resistance (F)			Ultimate values		
	f_{vk0} (MPa)	σ_0 (MPa)	$V_{exp,avg}$ (kN)	V_{Ed} (kN)	M_{Ed} (kNm)	$l_{c,linear}$ (mm)	σ_d (MPa)	f_{vk} (MPa)	$V_{Rd,s1}$ (kN)	f_b (MPa)	f_{vt} (MPa)	$V_{Rd,s2}$ (kN)	f_k (MPa)	M_{Rd} (kNm)	$V_{Rd,f}$ (kN)	$V_{Rd,u}$ (kN)	$V_{Rd,u}/V_{exp,avg}$ (kN)	Failure type
TTN	0.20	0.5	41.3	33.4	40.1	346.1	1.73	0.89	42.7	10.76	0.70	33.4	3.34	40.9	34.1	33.4	0.81	F + DS
TAND	0.12	0.5	37.8	29.9	32.2	651.6	0.92	0.49	44.5	5.04	0.33	29.9	2.57	38.9	36.2	29.9	0.79	DS
PPG	0.21	0.5	41.9	36.1	41.0	316.3	1.90	0.86	37.7	18.39	0.83	36.1	5.14	44.0	38.8	36.1	0.86	F + DS
PAND	0.06	0.5	39.3	25.3	28.1	798.1	0.75	0.33	37.0	5.04	0.23	25.3	2.57	38.9	35.0	25.3	0.64	DS
PAND*	0.06	0.5	39.3	29.3	32.5	639.4	0.94	0.44	39.0	5.04	0.33	29.3	2.57	38.9	35.0	29.3	0.75	DS

*Calculations made considering filled head joints in the PAND specimens for comparison purposes

Table 6. Analytical results according to EN 1996-1-1 assuming $l_{c,uniform} = 2 \left(\frac{l}{2} - e \right)$

Specimens	Experimental values			Sliding shear (SS)						Diagonal shear (DS)			Flexural resistance (F)			Ultimate values		
	f_{vk0} (MPa)	σ_0 (MPa)	$V_{exp,avg}$ (kN)	V_{Ed} (kN)	M_{Ed} (kNm)	$l_{c,uniform}$ (mm)	σ_d (MPa)	f_{vk} (MPa)	$V_{Rd,s1}$ (kN)	f_b (MPa)	f_{vt} (MPa)	$V_{Rd,s2}$ (kN)	f_k (MPa)	M_{Rd} (kNm)	$V_{Rd,f}$ (kN)	$V_{Rd,u}$ (kN)	$V_{Rd,u}/V_{exp,avg}$ (kN)	Failure type
TTN	0.20	0.5	41.3	30.5	36.6	316.2	1.90	0.96	41.8	10.76	0.70	30.5	3.34	40.9	34.1	30.5	0.74	DS
TAND	0.12	0.5	37.8	25.3	27.2	552.5	1.09	0.55	42.9	5.04	0.33	25.3	2.57	38.9	36.2	25.3	0.67	DS
PPG	0.21	0.5	41.9	33.2	37.7	290.4	2.07	0.93	37.3	18.39	0.83	33.2	5.14	44.0	38.8	33.2	0.79	DS
PAND	0.06	0.5	39.3	20.7	23.0	652.7	0.92	0.40	36.3	5.04	0.23	20.7	2.57	38.9	35.0	20.7	0.53	DS

Table 7. Analytical results according to EN 1996-1-1 assuming $l_{c,discrete} = \min(l_{c,linear}, l_u = \text{length of a masonry unit})$

Specimens	Experimental values			Sliding shear (SS)						Diagonal shear (DS)			Flexural resistance (F)			Ultimate values		
	f_{vk0} (MPa)	σ_0 (MPa)	$V_{exp,avg}$ (kN)	V_{Ed} (kN)	M_{Ed} (kNm)	$l_{c,discrete}$ (mm)	σ_d (MPa)	f_{vk} (MPa)	$V_{Rd,s1}$ (kN)	f_b (MPa)	f_{vt} (MPa)	$V_{Rd,s2}$ (kN)	f_k (MPa)	M_{Rd} (kNm)	$V_{Rd,f}$ (kN)	$V_{Rd,u}$ (kN)	$V_{Rd,u}/V_{exp,avg}$ (kN)	Failure type
TTN	0.20	0.5	41.3	27.8	33.4	288.0	2.08	1.03	41.1	10.76	0.70	27.8	3.34	40.9	34.1	27.8	0.67	DS
TAND	0.12	0.5	37.8	27.5	29.6	600.0	1.00	0.52	43.7	5.04	0.33	27.5	2.57	38.9	36.2	27.5	0.73	DS
PPG	0.21	0.5	41.9	36.1	41.0	315.9	1.90	0.86	37.7	18.39	0.83	36.1	5.14	44.0	38.8	36.1	0.87	DS
PAND	0.06	0.5	39.3	19.1	21.2	600.0	1.00	0.43	36.1	5.04	0.23	19.1	2.57	38.9	35.0	19.1	0.48	DS

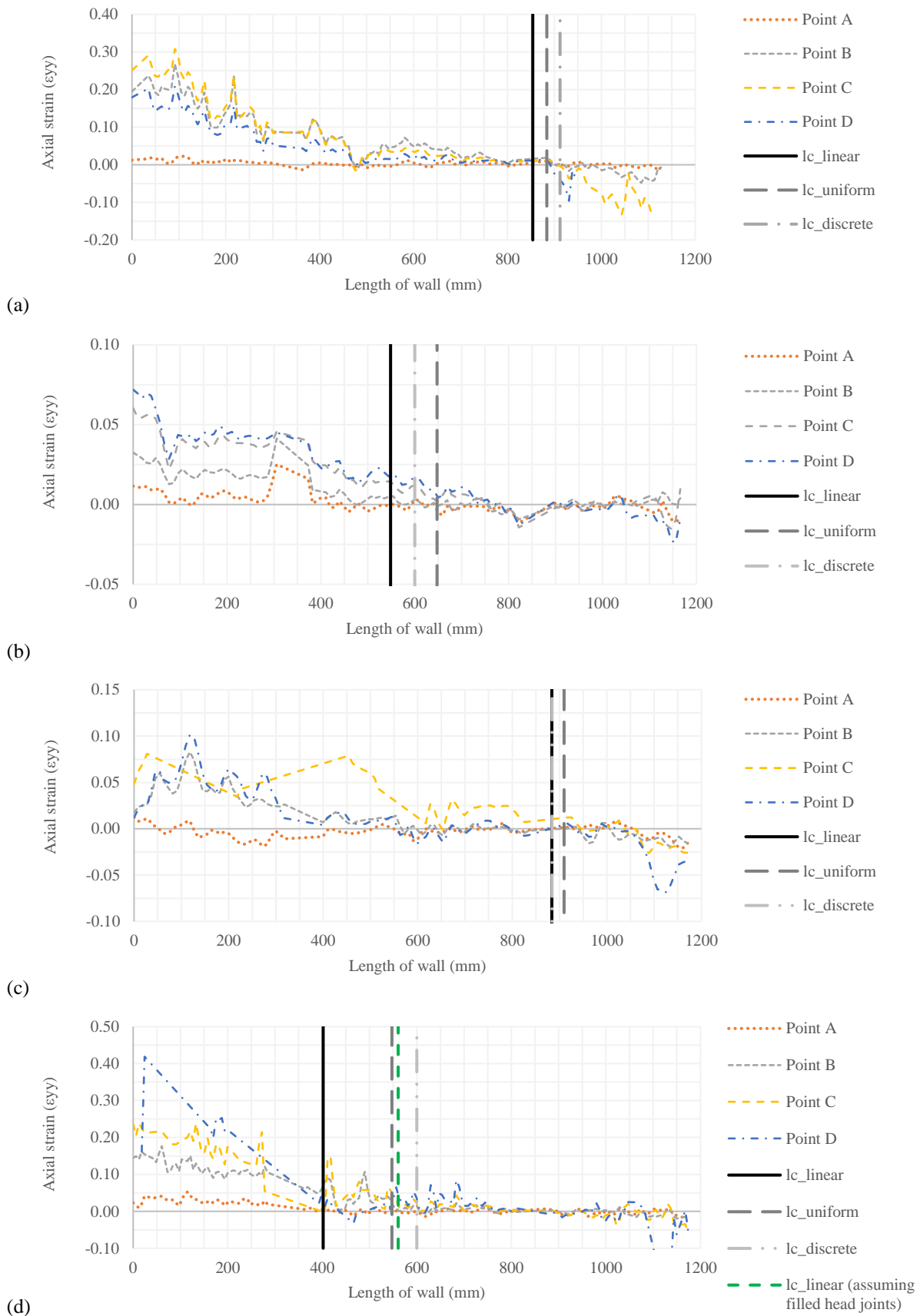


Figure 19. Comparison between the experimental and analytical axial strains at the bottom and along the length of the wall for specimens (a) TTN1, (b) TAND2, (c) PPG2 and (d) PAND1.

3.3.3 Considerations on the effective shear span ratio

The experiments were designed to test the wall specimens in a pure cantilever configuration, and therefore a shear span ratio equal to 1.0 was considered for the analytical calculations listed in Tables 5 to 7. However, many past researches have stated the uncertainty regarding the shear span ratio during experimental investigations, which can influence the ultimate failure mode of the masonry walls. Concerning this aspect, additional calculations were carried out in order to assess the influence of the shear-span ratio on the in-plane lateral resistance and the failure mode of the tested wall specimens. The shear span ratio was varied from 0.5 to 1.0 corresponding to a fixed-fixed and a free-fixed boundary condition at the top and bottom of the wall. The lateral resistance values, $V_{Rd,s1}$, $V_{Rd,s2}$ and $V_{Rd,f}$ corresponding to the different failure mechanisms, respectively sliding shear, diagonal shear cracking and flexural failure, are compared to evaluate the transition between the different failure mechanisms (see Fig. 20) with respect to the shear span.

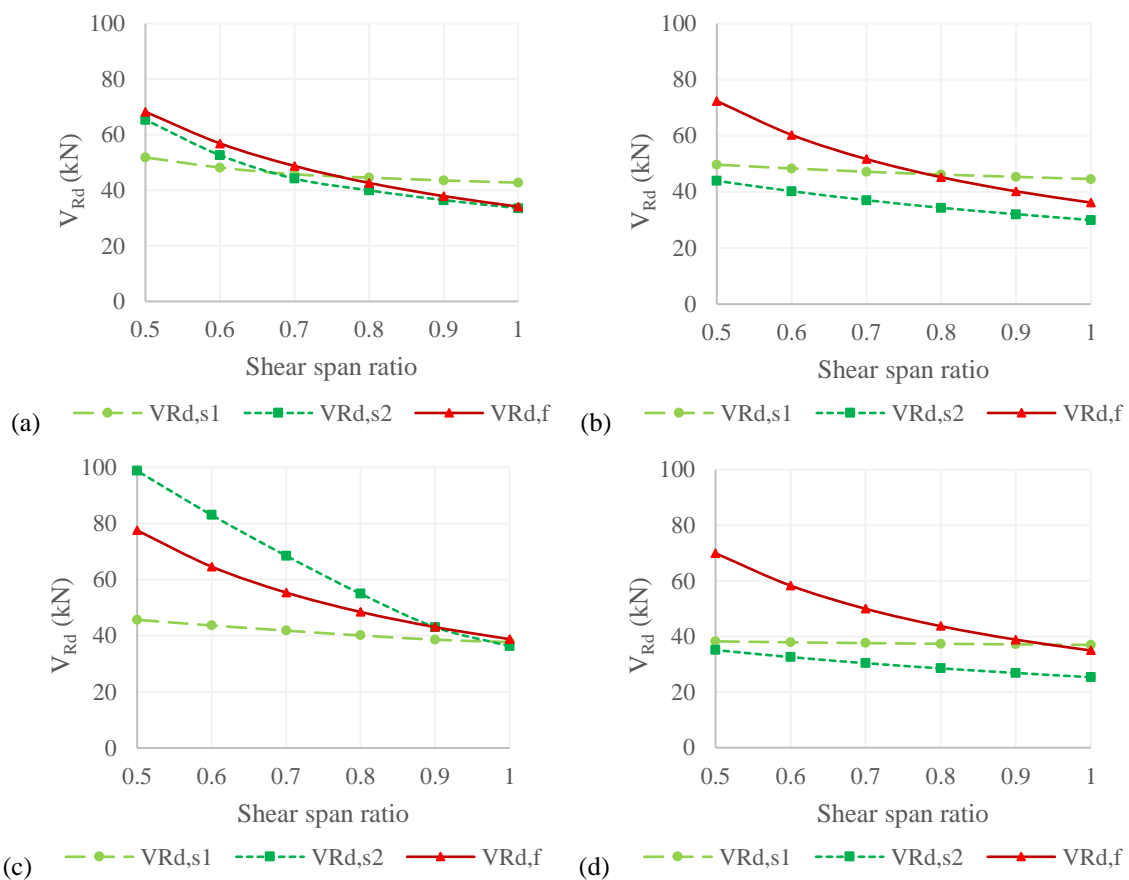


Figure 20. Influence of the shear span ratio on the in-plane behaviour of the specimens (a) TTN, (b) TAND, (c) PPG and (d) PAND.

It can be noticed that with an increasing shear span ratio, the failure mode for a TTN specimen shifts from a sliding shear failure to a combined toe crushing failure due to flexure and diagonal shear cracking – which has already been observed from the experiments (shear span ratio = 1). The PPG specimens indicates a slightly different behaviour, where all three failure modes tend to converge together for a higher shear span ratio. However, for the specimens with an AAC and DPC layer, i.e. TAND and PAND, the ultimate failure mode is always predicted to occur due to diagonal shear cracking for the varying shear span ratios, which essentially leads to a toe crushing failure as observed during the experiments. The primary reason behind this is the lack of compressive

strength of the AAC units. However, it should also be noted that, even if the shear span ratio undergoes marginal deviation during the experiments, i.e. from its controlled value ($= 1$) to a range of 0.9 - 1.0, due to some unforeseen uncertainties in the support fixities or the load introduction set-up, it will not have any impact on the conclusions drawn regarding the failure patterns of the different specimens.

4. Conclusions

This paper presents experimental investigations conducted on twelve masonry walls built up with traditional clay masonry units and different types of mortar (GPM and TLM), including or not a thermal break element (AAC) layer and a damp-proof course layer (DPC), subjected to a combination of horizontal and vertical loading conditions. The shear behaviour of traditional masonry walls (i.e. without AAC and DPC layers) were compared with the composite masonry walls in order to characterize the influence of the AAC and DPC layers on the shear behaviour of the walls. An analytical approach according to EN 1996-1-1 was also derived and compared to the experimental results to assess its applicability for the composite walls.

The following conclusions can be drawn from the experimental observations. The presence of thermal break elements (AAC) and DPC layer leads to up to approximately 8% reduction of the in-plane shear strength of the wall specimens. While the DPC layer reduces the friction and consequently the sliding shear strength of the wall specimens, the AAC layer adversely affects the flexural and diagonal shear strength of the wall due to its lower compressive strength. A loss of stiffness is also noticed. The failure mechanism is observed to be different for the composite specimens compared to the traditional ones. While the masonry walls without AAC and DPC fail due to a combination of flexural toe crushing and diagonal shear sliding, the walls with AAC and DPC layers fail due to a toe crushing of the AAC layer. A significant amount of horizontal shear sliding is also noticed in the latter cases at the joint above the DPC layer. Furthermore, the experimental evolution of axial strains shows that the traditional masonry walls exhibit an uplift only at the bottom of the wall specimens. On the other hand, uplift occurs at two different bed joints for the composite specimens, following the increase of the horizontal load applied at the top of the wall – (i) at the bottom of the wall specimens, starting from low load levels and (ii) between the first and the second layer of the wall specimens (location of the DPC) from a higher load level.

The mortar type is also observed to influence the post-peak behaviour of the masonry walls, independently of the presence of AAC and DPC. Once the maximum resistance is reached, a sudden drop in strength is noticed for the traditional walls with thin layered mortar (TLM) instead of a gradual reduction of strength, as observed in case of the wall specimens with general purpose mortar (GPM). This occurs due to the brittle nature and the limited thickness of the TLM, which activates the diagonal shear sliding behaviour in a rather sudden and abrupt manner compared to the GPM specimens.

It is however clear that those conclusions have to be considered as partial, as obtained in a specific scope, i.e. quasi-square wallettes of limited height, a shear-span ratio close to 1, a moderate initial compression level of 0.5 N/mm², perforated clay units of two formats and a rather high nominal compression resistance. Extending the experimental database beyond this scope constitutes thus an interesting perspective for future researches. In particular, more slender walls characterized by a more pronounced flexure behaviour or a lower initial compression load would be interesting extensions in view of the practical application context, as it is likely to change completely the mechanism inducing the failure and the triggering of the toe crushing.

The analytical calculation procedure proposed by the European standards offered good predictions for the traditional wall specimens without the AAC and DPC layers. It successfully predicts the maximum ultimate resistance and the active compressive length at ultimate limit state of the wall specimens and their corresponding failure modes with a realistic safety margin ($\approx 19\%$ on the resistance). However, similar conclusions could not be drawn for the composite wall specimens with the AAC and DPC layers, especially for the specimens with unfilled vertical head joints between the clay bricks. A straightforward quantification assuming either filled or unfilled head joints, as proposed by EN 1996-1-1, becomes indeed complicated since, when thermal break elements are used, it is quite often the case that the vertical head joints between the AAC units are filled while the head joints of the clay bricks layer on top of it are actually unfilled. In such cases, although the clay bricks build up to 90% of the walls, the failure mechanism is essentially governed by the AAC layer located at the bottom of the wall. Therefore, considering such composite walls to be with unfilled head joints and consequently using a 0.5 reduction factor for the initial (sliding) shear strength or the $0.045f_b$ limit for the diagonal shear strength leads to a significant underestimation of the in-plane shear strength of the wall. Moreover, along with these design limits, the EN 1996-1-1 design approach assumes that the wall consists 100% of the weakest material (e.g. AAC), which pushes towards an even more conservative design. In conclusion, it appears that the most accurate EN 1996-based design approach consists in considering for the entire verification the type of vertical joints of the weakest layer, although a mixed approach could be investigated in further researches. Moreover, the favourable stiffening effect of the clay units on the AAC layer is a point that would deserve further investigation to reduce the conservatism of the analytical predictions. It was also noted that, while the shear span ratio might have a relevant influence on determining the failure mechanism in a traditional masonry wall, it does not have a significant impact on the masonry walls with an AAC and DPC layer.

Nevertheless, it should be highlighted that only a single layer of AAC and DPC were considered for this study. A comprehensive analytical assessment is necessary along with complimentary tests with multiple layer(s) of AAC units, to understand their influence in a more detailed manner and then to further characterize the EN 1996-1-1 design limits for composite masonry walls with thermal and damp-proof course layers under in-plane shear loads.

Author contributions: Dan Dragan: Investigation (experimental), Data curation, Software; Rajarshi Das: Data curation, Investigation (analytical), Validation, Writing – original draft; Martijn Vanheukelom: Data curation, Investigation (experimental); Bram Vandoren: Supervision, Conceptualization, Methodology, Reviewing and Editing; Herve Degee: Supervision, Conceptualization, Methodology, Reviewing and Editing.

Funding: Part of this research was funded by the VLAIO TETRA project InnoMaso: HBC.2018.0053.

Data Availability Statement: The data presented in this study are available on request from the corresponding author. The data are not publicly available due to the fact that it is part of an ongoing research.

Conflicts of Interest: The authors declare no conflict of interest.

References

- [1] D. Ferretti, E. Michelini, G. Rosati. Cracking in autoclaved aerated concrete: Experimental investigation and XFEM modeling. *Cement and Concrete Research* 67 (2015) 156–167.
- [2] M. Deyazada, B. Vandoren and H. Degee. Structural resistance and stability of masonry walls with thermal break elements. Doctoral Thesis, Hasselt University, Belgium, 2021.
- [3] EN 772-1. Methods of test for masonry units. Part 1: Determination of compressive strength. European Committee for Standardization. Brussels, Belgium, 2011.
- [4] EN 1052-1. Methods of test for masonry. Part 1: Determination of compressive strength. European Committee for Standardization. Brussels, Belgium, 1998.
- [5] EN 1996-1-1. Eurocode 6 - Design of masonry structures - Part 1-1: General rules for reinforced and unreinforced masonry structures. European Committee for Standardization. Brussels, Belgium, 2021.
- [6] WTCB, Thermische isolatie van bestaande muren, 2016.
- [7] V. I. Bio-Ecologisch Bouwen en Wonen (VIBE), Bio-ecologisch bouwen, 2016.
- [8] L. Malyszko, E. Kowalska and P. Bilko. Splitting tensile behavior of autoclaved aerated concrete: Comparison of different specimens' results. *Construction and Building Materials*, 157 (2017) 1190-1198.
- [9] D. Ferretti, E. Michelini, G. Rosati. Cracking in autoclaved aerated concrete: Experimental investigation and XFEM modeling. *Cement and Concrete Research* 67 (2015) 156–167.
doi: 10.1016/j.cemconres.2014.09.005.
- [10] A. M. Memari, S. V. Grossenbacher and L. D. Iulo. Structural testing of high thermal mass walls used in sustainable designs. In *Structures Congress 2008, Crossing Borders*.
- [11] A. M. Papadopoulos. State of the art in thermal insulation materials and aims for future developments. *Energy and Buildings* 37 (2005) 77-86.
- [12] N. Narayanan and K. Ramamurthy. Structure and properties of aerated concrete: a review. *Cement and Concrete composites* 22 (2000) 321-329.
- [13] M. Gams. Seismic behaviour of confined autoclaved aerated concrete masonry buildings: a shaking table study. *Mauerwerk* 14 (2010) 153-160.
- [14] B. Trunk, G. Schober, A. K. Helbling and F. H. Wittmann. Fracture mechanics parameters of autoclaved aerated concrete. *Cement and Concrete Research* 29 (1999) 855-859.
- [15] C. A. Snow. A comprehensive study of the material properties and structural behavior of AAC products. 1999.
- [16] F. H. Fouad and J. Dembowski. Mechanical Properties of Plain AAC Material. American Concrete Institute, Special Publication 226 (2005) 1-16. doi: 10.14359/14388.
- [17] M. C. Limbachiya and J. J. Roberts. *Autoclaved aerated concrete: innovation and development*. Taylor & Francis, 2005.
- [18] M. Graubohm and W. Brameshuber. Crack safety of non-load partition walls made of autoclaved aerated concrete. In *9th International Masonry Conference, Guimaraes*, 2014.
- [19] B. Foamglas. My New Favourite Insulation Material. 2016.
- [20] R. Jasinski, T. Gasiorowski. Comparative studies of the confined effect of shear masonry walls made of autoclaved aerated concrete masonry units. *Materials* 16 (2023) 5885. <https://doi.org/10.3390/ma16175885>

- [21] R. Jasinski. Verifying the shear load capacity of masonry walls by the $V_{Rd}-N_{Ed}$ interaction diagram. IOP Conf. Series, Materials Science and Engineering 1203 (2021) 022031. doi:10.1088/1757-899X/1203/2/022031
- [22] D. Martens. Thermal break with cellular glass units in load bearing masonry walls. IMS: International Masonry Society, 2014.
- [23] M.C. Griffith and A.W. Page. On the seismic capacity of typical DPC and slip joints in unreinforced masonry buildings. Australian Journal of Structural Engineering (1998) 1(2): 133–40.
- [24] G. Simundic, A.W. Page, Q. Chen. The cyclic and long-term behaviour of slip joints in load-bearing masonry construction. In: Proceedings of the 12th International brick/block masonry conference, Madrid, 2000. pp. 1409–20.
- [25] Y. Totoev, A.W. Page, G. Simundic. Shear transfer capacities of horizontal slip joints in masonry at different levels of vertical load. In: Proceedings of the 9th North American masonry conference, Clemson, 2003. pp. 791–800.
- [26] Y. Totoev, G. Simundic. New test for the shear transfer capacity of horizontal slip joints in load-bearing masonry. In: Proceedings of the 10th Canadian masonry symposium, Banff, 2005. pp. 863–72.
- [27] G.T. Suter, K.S. Ibrahim. Shear resistance of damp-proof-course materials in brick-mortar joints. In: Proceedings of the 6th Canadian masonry symposium, Saskatoon, 1992. pp. 119–30.
- [28] Y. Zhuge, J. Mills. The behaviour of masonry walls containing a damp-proof course under cyclic loads. In: Proceedings of the 2nd Australasian structural engineering conference, Auckland, 1998. pp. 655–61.
- [29] M. Petrovic, N. Mojsilovic, B. Stojadinovic. Masonry walls with a multi-layer bed joint subjected to in-plane cyclic loading: An experimental investigation. Engineering Structures 143 (2017) 189–203. <https://doi.org/10.1016/j.engstruct.2017.04.025>.
- [30] C. Vogeli, N. Mojsilovic, B. Stojadinovic. Masonry wallets with a soft layer bed joint: Behaviour under static cyclic loading. Engineering Structures 86 (2015) 16–32. <https://doi.org/10.1016/j.engstruct.2014.12.038>.
- [31] M. Tomazevic. Earthquake-Resistant Design of Masonry Buildings. World Scientific, 1999.
- [32] G. Magenes and G. M. Calvi. In-plane seismic response of brick masonry walls. Earthquake Engineering & Structural Dynamics 26 (11) (1997) 1091–1112. [https://doi.org/10.1002/\(SICI\)1096-9845\(199711\)26:11<1091::AID-EQE693>3.0.CO;2-6](https://doi.org/10.1002/(SICI)1096-9845(199711)26:11<1091::AID-EQE693>3.0.CO;2-6)
- [33] A. H. Salmanpour, N. Mojsilovic, and J. Schwartz. Displacement capacity of contemporary unreinforced masonry walls: an experimental study. Engineering Structures 89 (2015) 1–16. <https://doi.org/10.1016/j.engstruct.2015.01.052>
- [34] M. Deyazada, B. Vandoren, D. Dragan, H. Degee. Experimental investigations on the resistance of masonry walls with AAC thermal break layer. Construction and Building Materials 224 (2019) 474–492. <https://doi.org/10.1016/j.conbuildmat.2019.06.205>.
- [35] M. Vanheukelom, R. Das, H. Degee and B. Vandoren. Experimental characterization of the initial shear strength of composite masonry including AAC blocks and DPC layers. Sustainability 13 (2021) 12749. <https://doi.org/10.3390/su132212749>
- [36] <https://www.wienerberger.be/fr/mur-interieur/choisissez-votre-bloc/thermobrick-10n.html>
- [37] <https://www.wienerberger.be/Binnenmuur/productzoeker/pls-500-15n.html>

- [38] NBN EN 1996-1-1 + A1 ANB. Eurocode 6 - Design and calculation of masonry structures - Part 1-1: Common rules for reinforced and unreinforced masonry structures - National Annex. Belgium, 2016.
- [39] M. Kaluza, J. Kubica. Behaviour of unreinforced and reinforced masonry wallettes made of ACC blocks subjected to diagonal compression. Technical Transactions. Department of Structural Engineering, Faculty of Civil Engineering, Silesian University of Technology, Gliwice.
https://suw.biblos.pk.edu.pl/resources/i4/i0/i5/i2/i2/r40522/KaluzaM_BehaviourUnreinforced.pdf